



OPEN

Rosmarinus officinalis L. hexane extract: phytochemical analysis, nanoencapsulation, and in silico, in vitro, and in vivo anti-photoaging potential evaluation

Nehal Ibrahim¹✉, Haidy Abbas², Nesrine S. El-Sayed³ & Heba A. Gad^{4,5}✉

A shift towards natural anti-aging ingredients has spurred the research to valorize traditionally used plants. In this context, *Rosmarinus officinalis* L. was evaluated for its photoprotective, antioxidant, anti-inflammatory, and anti-wrinkling properties. GC/MS and LC-ESI-HRMS based phytochemical profiling of rosemary leaves hexane extract resulted in the identification of 47 and 31 compounds, respectively and revealed rich content in triterpenoids, monoterpenoids and phenolic diterpenes. In vitro assays confirmed the antioxidant, anti-aging, and wound healing potential of rosemary extract along with a good safety profile, encouraging further development. A systematic molecular modelling study was conducted to elucidate the mechanistic background of rosemary anti-aging properties through the inhibitory effects of its major constituents against key anti-aging targets viz. elastase, collagenase, and hyaluronidase. Development of rosemary extract lipid nanocapsules-based mucoadhesive gels was performed to improve skin contact, permeation, and bioavailability prior to in vivo testing. The developed formulae demonstrated small particle size (56.55–66.13 nm), homogenous distribution (PDI of 0.207–0.249), and negatively charged Zeta potential (– 13.4 to – 15.6). In UVB-irradiated rat model, topical rosemary hexane extract-loaded lipid nanocapsules-based gel provided photoprotection, restored the antioxidant biochemical state, improved epidermal and dermal histological features, and decreased the level of inflammatory and wrinkling markers. The use of rosemary hexane extract in anti-aging and photoprotective cosmeceuticals represents a safe, efficient, and cost-effective approach.

Skin aging is a multifactorial physiological and pathophysiological phenomenon affected by genetic, hormonal, metabolic, and environmental factors. Since skin is constantly exposed to the environment, combatting skin damage due to the solar UV radiation has been gaining considerable interest especially with the increase in human life expectancy. Repeated exposure to solar UV radiation results in cleavage and disorganization of skin connective tissue with subsequent sagging and appearance of crevices and wrinkles. In addition, skin aging is accompanied with impaired wound healing and pigmentation changes¹.

Due to consumers' growing concerns about synthetic products and their possible detrimental health effects, there has been a shift during the last decades towards the implementation of natural bioactive, functional ingredients or additives in cosmetics and personal care products^{2–5}. Such preference for natural cosmeceuticals is maximized when they are derived from edible sources and culinary herbs^{4,6} and was reflected on the European

¹Pharmacognosy Department, Faculty of Pharmacy, Ain Shams University, Cairo 11566, Egypt. ²Pharmaceutics Department, Faculty of Pharmacy, Damanhour University, Damanhour, Egypt. ³Pharmacology and Toxicology Department, Faculty of Pharmacy, Cairo University, Cairo, Egypt. ⁴Pharmaceutics and Industrial Pharmacy Department, Faculty of Pharmacy, Ain Shams University, Cairo 11566, Egypt. ⁵Department of Pharmaceutical Sciences, Pharmacy Program, Batterjee Medical College, Jeddah, Saudi Arabia. ✉email: nehal.sabry@pharma.asu.edu.eg; h.gad@pharma.asu.edu.eg

market of natural cosmetics which was valued at 4 billion dollars in 2015 and further expanded globally between 2015 and 2019, with up to 11% annual growth^{3,4,7}. Many of such natural ingredients exhibit antioxidant, anti-inflammatory, and antimicrobial properties. Rosemary (*Rosmarinus officinalis* L.) is a Lamiaceae shrub widely distributed in the Mediterranean region where its use dates back to the pharaonic era⁸. The ancient Egyptians used rosemary together with chamomile, myrrh, and thyme to protect skin against desert heat⁹. In addition, *R. officinalis* has long history of use in phytotherapeutic traditions as antispasmodic, diuretic, antirheumatic, and antiepileptic, and showed effectiveness in treating respiratory problems and skin infections and enhancing wound healing⁸. Moreover, during the World War II, rosemary leaves were burnt to disinfect hospitals¹⁰.

Recently, a plethora of biological activities have been reported to rosemary essential oils and to the polar phenolics extracts (prepared by methanol, ethanol, and acetone), including antioxidant, anti-inflammatory, hypoglycemic, antimicrobial, hepato-, nephro-, and neuroprotective, memory enhancing, wound healing, and anti-wrinkle properties, validating many of its traditional uses^{11–19}. All these activities were attributed to rosemary's complex repertoire of volatile constituents, phenolic diterpenes, e.g., carnosol and carnosic acid; and polyphenols, e.g., rosmarinic acid^{11,13,19–22}. Nevertheless, quite surprisingly less interest has been paid to rosemary hexane extracts compared with the large body of literature available on rosemary essential oil and alcoholic extracts^{10–12,20,23,24}. A lot of research has been conducted and published on rosemary essential oil or alcoholic extracts while the hexane extracts with their uniquely different composition remain much less explored. Previous studies have documented the superior antioxidant activity and higher carnosic acid content of rosemary hexane extract compared with rosemary phenolics extracts prepared with methanol, ethanol, and acetone^{23,24}. In addition, hexane efficiently extracts the aroma compounds, e.g., monoterpenes, sesquiterpenes, phenylpropanes, and their oxygenated derivatives which may exhibit antioxidant and antiaging properties^{25–27} and further improve consumer acceptability. Furthermore, unlike polar solvents, hexane can extract triterpenes which exhibit anti-inflammatory properties²⁸, tocopherols, and saturated and unsaturated fatty acids which exhibit anti-inflammatory, antioxidant, antiaging, and permeation enhancing effects^{29,30}. However, *R. officinalis* hexane extract is regarded as a byproduct during the agri-food processing of rosemary for the production of decolorized polyphenol-rich extracts for commercial exploitation as natural antioxidants and antimicrobials in food preservation. This results in the generation of significant volumes of hexane extract wastes³¹. With the initiative of circular economy, such wastes can be valuable sources of phytochemicals needed in different industrial and medicinal applications, which necessitates their valorization to render the process more sustainable and maximize economic and environmental benefits^{5,31,32}.

Lipid nanocapsules (LNC) are newly evolved lipid-based nanocarriers formed of an oily core of medium chain triglycerides that is enclosed within a shell of PEGylated surfactant and lipoid. The oily core of LNC increases their ability to encapsulate lipophilic compounds. In addition, their small particle size (20–100 nm) grants high skin permeation upon dermal application. Other advantages include safety, biocompatibility, ease of preparation, and good stability^{33,34}.

The present work is undertaken to unveil the compositional profile, the in vitro anti-aging, antioxidant, and wound healing potentials as well as the cytotoxic effect of *Rosmarinus officinalis* L. hexane extracts, and to improve its skin permeation and bioavailability through inclusion into lipid nanocapsules-based gel. In addition, the cosmeceutical potential of formulated and unformulated *R. officinalis* hexane extract was evaluated in vivo with regard to its UV-protection capacity and antioxidant, anti-inflammatory, and anti-wrinkling properties. Moreover, a systematic molecular modelling study was conducted to elucidate the mechanistic background of the anti-aging properties of rosemary hexane extract.

Results and discussion

Chemical profiling of *R. officinalis* hexane extract. *GC-MS analysis.* GC-MS analysis was implemented to assess the metabolite composition of rosemary hexane extract (RHE) revealing the presence of monoterpenes, their oxygenated derivatives, sesquiterpenes, long chain alkanes, and triterpenoids and resulting in the identification of 47 components representing 99.29% of detected peaks (Table 1). Triterpenes (45.2%) and hydrocarbons (41.8%) dominated the extract with α -amyrin, dotriacontane, β -amyrin, and triacontane as major components. Volatile constituents of rosemary aroma were mainly represented by monoterpenes and their oxygenated derivatives detected at 3% and 8.4%, respectively. The chief monoterpene was α -pinene, while the major oxygenated monoterpenes included the ketones verbenone and camphor, besides 1,8-cineole and borneol. This is congruent with previous reports of major terpenes of rosemary essential oil¹¹. Lipophilic hexane extracts of aromatic plants exhibit aroma profile that closely mimics the characteristic odour of fresh plant. On the contrary, the aroma quality of volatiles prepared by distillation may differ from the fresh raw material because of the high temperatures used in distillation procedures^{36,37}.

Triterpenoids were dominated by α -amyrin (24.4%), β -amyrin (14.4%), and lupeol acetate (4.9%). α -Amyrin, a pentacyclic triterpene alcohol previously identified as minor component in *R. officinalis* ethanol extract³⁸, showed anti-inflammatory, anti-allergic, antihyperlipidemic, and anti-ulcer activities^{39–42}. In vitro, this triterpenoid stimulated human keratinocytes proliferation⁴³. Lupeol acetate demonstrated anti-inflammatory, antinociceptive, and anti-arthritic activities^{44,45}.

LC-ESI-HRMS analysis. *Rosmarinus officinalis* leaves hexane extract was profiled for its phytochemical composition using LC-ESI-HRMS. The compounds were tentatively identified by comparing their corresponding retention times and HRMS data with those previously reported in literature and online databases. The LC-ESI-HRMS analysis resulted in the tentative identification of 31 metabolites from different classes. Phenolic diterpenes (e.g., rosmanol, carnosol, carnosic acid, and rosmadial) represent the most abundant class detected in RHE with 14 identified compounds in accordance with previous studies^{46,47}, followed by triterpenoids (e.g., betulonic,

No	RT (min)	RI exp ^a	RI lit ^b	Metabolite ^c	Relative percentile
1	7.07	914	914	α -Pinene	1.73
2	7.52	929	929	Camphene	0.46
3	7.7	936	937	2,4(10)-Thujadiene	0.1
4	8.39	960	960	β -Pinene	0.13
5	9.45	998	998	δ 3-carene	0.08
6	9.93	1013	1013	<i>p</i> -Cymene	0.07
7	10.05	1017	1017	Limonene	0.4
8	10.11	1019	1019	Eucalyptol	1.63
9	12.34	1089	1089	Linalool	0.45
10	13.73	1133	1133	Camphor	2.07
11	14.32	1152	1152	Pinocarvone	0.12
12	14.42	1155	1155	Borneol	1.07
13	14.68	1163	1162	Isopinocampnone	0.17
14	15.22	1180	1180	α -Terpineol	0.21
15	15.59	1192	1196	Isoborneol	0.09
16	15.77	1198	1198	Verbenone	2.08
17	16.78	1233	1234	<i>cis</i> -Myrtanol	0.21
18	18.02	1276	1276	Bornyl acetate	0.31
19	21.8	1408	1408	Caryophyllene	0.2
20	42.19	2368	2300	Tricosane	0.21
21	43.84	2467	2400	Tetracosane	0.27
22	44.78	2528	2525	Diisooctyl phthalate	0.19
23	45.42	2569	2500	Pentacosane	0.43
24	46.93	2666	2600	Hexacosane	0.8
25	48.39	2760	2700	Heptacosane	0.65
26	49.83	2853	2800	Octacosane	3.07
27	51.18	2939	2865	2-methyloctacosane	0.9
28	52	2992	2965	2-Methylnonacosane	0.35
29	52.53	3026	3000	Triacontane	6.73
30	53.29	3075	3112	α -Tocopherol	0.34
31	53.49	3087	3015	3,7-dimethyl-nonacosane	0.54
32	53.83	3110	3100	Hentriacontane	1.34
33	54.58	3157	3120	n-Octacosanol	0.21
34	54.73	3167	3100	Hentriacontane	1.26
35	55.36	3208	3200	Dotriacontane	16.21
36	56.34	3270	3225	16-Methyldotriacontane	0.36
37	56.56	3285	3235	12-Methyldotriacontane	1.7
38	56.69	3294	3337	β -Amyrin	10.4
39	56.99	3313	3300	Tritriacontane	1.11
40	57.1	3319	3337	β -Amyrin	3.95
41	57.57	3350	3376	α -Amyrin	20.64
42	58	3377	3376	α -Amyrin	3.79
43	58.19	3389	3338	15-Methyltritiacontane	0.71
44	58.98	3440	3400	Tetatriacontane	5.11
45	59.35	3464	3384	Lupenone	0.67
46	62.4	3660	3525	Lupeol acetate	4.91
47	62.62	3674	3629	Betulinolaldehyde	0.86
% Total Identified					99.29
% Monoterpenes					2.97
% Oxygenated monoterpenes					8.41
% Sesquiterpenes					0.2
% Hydrocarbons					41.75
% Triterpenoids					45.22
Others					0.74

Table 1. Compositional profile of *R. officinalis* hexane extract as analysed by GC-MS. ^aRetention index calculated experimentally on Rtx-5MS column relative to C8-C28 n-alkanes series. ^bCorresponding Kovats retention index from literature and spectral databases. ^cIdentification based on comparing retention indices (RI) and mass spectral data (MS) with those found in NIST Mass Spectral Library (2011), Wiley Registry of Mass Spectral Data (8th edition) and reported in literature.

No	RT (min)	Annotation	Molecular formula	Exp. [M-H] ⁻ m/z	Exact mass	MS/MS	Error (ppm)	Class	Refs.
1	19.234	Coniferyl alcohol	C ₁₀ H ₁₂ O ₃	179.0712	180.0786	nd	0.49	Phenylpropanoid	52
2	26.094	Podolide	C ₁₉ H ₂₂ O ₅	329.1405	330.1467	nd	-4.28	Norditerpene	53
3	29.12	Rosmanol	C ₂₀ H ₂₆ O ₅	345.1717, 691.3501 [2 M-H] ⁻	346.178	283, 301	-1.76	Phenolic diterpene	46,47
4	30.331	(Epi)(iso)rosmanol I	C ₂₀ H ₂₆ O ₅	345.1718, 691.3507 [2 M-H] ⁻	346.178	283, 301	-3.09	Phenolic diterpene	46,49
5	31.441	(Epi)(iso)rosmanol II	C ₂₀ H ₂₆ O ₅	345.1719	346.178	283, 301	-3.14	Phenolic diterpene	46
6	34.568	Lariciresinol	C ₂₀ H ₂₄ O ₆	359.1509	360.1573	nd	-2.48	lignan	54
7	35.072	Unidentified	C ₁₉ H ₂₂ O ₄	313.1452	314.1518	nd	-2.15		
8	36.485	Rosmadiol	C ₂₀ H ₂₄ O ₅	343.1563, 687.3191 [2 M-H] ⁻	344.1624	299, 315, 313	-3.34	Phenolic diterpene	47
9	37.494	(Epi)rosmanol methyl ether	C ₂₁ H ₂₈ O ₅	359.1877	360.1937	344, 315, 329	-3.36	Phenolic diterpene	46,55
10	38.099	Carnosol	C ₂₀ H ₂₆ O ₄	329.1772, 659.3604 [2 M-H] ⁻	330.1831	285	-3.95	Phenolic diterpene	56,57
11	39.713	Rosmadiol isomer	C ₂₀ H ₂₄ O ₅	343.1565	344.1624	299, 315	-3.71	Phenolic diterpene	47
12	40.621	Unidentified	C ₁₉ H ₃₄ O ₄	325.2395	326.2457	nd	-2.94		
13	40.722	Rosmaridiphenol	C ₂₀ H ₂₈ O ₃	315.1977, 631.4020 [2 M-H] ⁻	316.2038	285, 135	-3.58	Phenolic diterpene	46
14	40.823	Carnosic acid	C ₂₀ H ₂₈ O ₄	331.1928, 663.3922 [2 M-H] ⁻	332.1988	244	-3.91	Phenolic diterpene	46,48,57
15	40.924	Rosmaridiphenol isomer I	C ₂₀ H ₂₈ O ₃	315.1980, 631.4024 [2 M-H] ⁻	316.2038	nd	-4.43	Phenolic diterpene	46
16	41.025	Rosmaridiphenol isomer II	C ₂₀ H ₂₈ O ₃	315.1977	316.2038	nd	-3.46	Phenolic diterpene	46
17	42.03	Unidentified	C ₂₃ H ₃₂ O ₃	355.2291	356.2351	nd	-3.21		
18	42.74	Carnosol isomer	C ₂₀ H ₂₆ O ₄	329.1770, 659.3601 [2 M-H] ⁻	330.1831	nd	-3.37	Phenolic diterpene	46,57
19	43.648	Asiatic acid	C ₃₀ H ₄₈ O ₅	487.3444, 975.6934 [2 M-H] ⁻	488.3502	nd	-2.95	Triterpenoid	58
20	45.06	12-O-methylcarnosic acid	C ₂₁ H ₃₀ O ₄	345.2080	346.2144	301	-2.85	Phenolic diterpene	47
21	45.665	Carnosic acid isomer	C ₂₀ H ₂₈ O ₄	331.1916	332.1988	nd	-0.38	Phenolic diterpene	46,57
22	47.3	Asiatic acid isomer	C ₃₀ H ₄₈ O ₅	487.3438	488.3502	nd	-2.29	Triterpenoid	
23	47.683	betulinic acid	C ₃₀ H ₄₈ O ₅	455.3543	456.3603	455, 411	-2.7	Triterpenoid	47,59
24	48.288	Lanopalmitic acid	C ₁₆ H ₃₂ O ₃	271.2283	272.2351	nd	-1.54	Hydroxy fatty acid	54
25	48.49	Unidentified triterpenoid	C ₃₀ H ₄₆ O ₃	453.3378	454.3447	nd	-0.73	Triterpenoid	
26	48.995	Oleanolic acid	C ₃₀ H ₄₈ O ₃	455.3537	456.3603	407	-1.25	Triterpenoid	47,59
27	50.810	Ursolic acid	C ₃₀ H ₄₈ O ₃	455.3540	456.3603	nd	-1.26	Triterpenoid	47,59
28	51.618	Unidentified triterpenoid	C ₃₀ H ₄₄ O ₃	451.3230, 903.6532 [2 M-H] ⁻	452.329	nd	-3.07	Triterpenoid	
29	52.626	Unidentified triterpenoid	C ₃₀ H ₄₆ O ₃	453.3390, 907.6833 [2 M-H] ⁻	454.3447	nd	-2.84	Triterpenoid	
30	59.89	Augustic acid	C ₃₀ H ₄₈ O ₄	471.3498	472.3553	nd	-2.79	Triterpenoid	55
31	72.298	Pyro-pheophytin-b	C ₅₃ H ₇₀ N ₄ O ₄	825.5338	826.5397	nd	-7.15	Chlorophyll derivative	60

Table 2. Phytochemical composition of *R. officinalis* hexane extract as analysed by LC-ESI-HRMS in negative ion mode.

oleanolic and ursolic acids) represented here by 9 compounds. The identified compounds and their chromatographic and HRMS data characteristics are depicted in Table 2.

Compounds 3, 4, 5, and 20 exhibited quasimolecular ions [M-H]⁻ at m/z 345. Compounds 3, 4, and 5 were tentatively identified as rosmanol, (epi)(iso)rosmanol I, and (epi)(iso)rosmanol II based on the accurate masses of the observed deprotonated quasimolecular ions (m/z 345.171) and deprotonated dimers [2 M-H]⁻ (m/z 691.3501). Additionally, fragment ions were detected at m/z 301, and 283 which correspond to the loss of CO₂ and sequential loss of CO₂ and water, respectively, in line with previously reported data for these isomeric compounds^{46,48}. Compound 20 was identified as 12-O-methylcarnosic acid. Although it showed the same nominal mass with [M-H]⁻ at m/z 345, it presented a different accurate mass of 345.2080 and eluted later in the chromatographic separation which is previously reported for 12-O-methylcarnosic acid^{48,49}. Fragment ion at m/z 301 indicated the loss of CO₂ from the carboxylic acid group⁴⁸.

Rosmadiol (compound 8) and its isomeric form (compound 11) showed quasimolecular ions at m/z 343.1563 and 343.1565, respectively. A unique fragmentation pattern was recorded for these compounds; loss of ethylene, CO₂ and HCHO can account for the product ions observed at m/z 315, 299 and 313, respectively, as formerly described^{46,48,49}. Compound 9 was identified as (epi)rosmanol methyl ether based on its [M-H]⁻ accurate mass

Sample	DPPH (IC ₅₀ , µg/mL)	ABTS (mM TE/g extract)	FRAP (mM TE/g extract)
RHE	221.6 ± 11.8	310.54 ± 12.32	394.69 ± 17.28
Trolox	6.11 ± 0.2	–	–

Table 3. Antioxidant activity of *R. officinalis* hexane extract.

of 359.1877 and its fragment ions at *m/z* 344, 329 and 315 attributed to loss of methyl, HCHO and CO₂⁵⁰. Carnosol (compound 10) as well as its isomer (compound 18) were identified based on the accurate masses of their [M-H][−] and [2 M-H][−] and the characteristic fragment ion at *m/z* 285 ascribed to the loss of CO₂. Rosmaridiphenol (compound 13) was identified based on the accurate mass of its [M-H][−] observed at *m/z* 315.1977 and its fragment ion at *m/z* 285, which is consistent with previous reports^{46,51}.

Carnosic acid (compound 14) and its isomer (compound 21) were identified by their corresponding deprotonated quasimolecular ions observed at *m/z* 331.1928 and 331.1916, respectively. Carnosic acid produced a fragment ion at *m/z* 244 which can be attributed to the loss of CO₂ + CH₃CH₂CH₂, as previously reported for this highly antioxidant phenolic diterpene^{48,49}.

In vitro antioxidant capacity. Oxidative stress is a key element in the aging process as well as in the aetiology of various chronic disorders through its inflammatory and degenerative consequences. Topical application of antioxidants can restore the balance between antioxidation and oxidation processes, prevent molecular damage, and maintain skin homeostasis. In this regard, plant extracts provide a wide range of antioxidant molecules ranging from phenolic acids, flavonoids, and tannins to carotenoids, tocopherols, and terpenoids. It is noteworthy that the extraction solvent has a strong impact on the antioxidant activity of a plant extract. Although polar solvents, e.g., methanol and ethanol, are best suited for extraction of polyphenols and better reflect the antioxidant potential of a plant⁶¹, the *n*-hexane extract of certain plants, including rosemary, demonstrated better antioxidant activity than their polar extracts based on *in vitro* chemical antioxidants tests^{23,24,62}.

The antioxidant activity was assessed using DPPH and ABTS free radicals scavenging assays as well as FRAP assay. RHE was able to scavenge DPPH radical (IC₅₀ of 221.6 ± 11.8 µg/mL), but it was less active than Trolox (IC₅₀ of 6.1 ± 0.2 µg/mL) (Table 3). The DPPH scavenging activity of RHE is comparable to *Ipomoea cairica* and *Bauhinia purpurea* hexane extracts⁶³. However, it is much less than the DPPH scavenging capacity of rosemary essential oil (IC₅₀ of 77.6 µL/mL)⁶⁴. Meanwhile, it is worth mentioning that this antioxidant activity is comparable and even superior to published antioxidant properties of phenolics rich extracts^{65,66}.

The free radical scavenging capacity of RHE was also evaluated using the ABTS decolorization assay. This is based on the capacity of antioxidant compounds to scavenge the radical cation ABTS^{•+} relative to the standard antioxidant Trolox. RHE demonstrated a Trolox equivalent antioxidant capacity of 310.5 ± 12.3 mM TE/g dry extract (Table 3), well above the previously reported antioxidant capacity of *Vitex agnus-castus* leaves and fruits hexane extract⁶⁷.

The FRAP assay is used to evaluate the reducing power of compounds and depends on the ability of antioxidants in plant extracts to reduce the colourless Fe³⁺-TPTZ complex to the blue coloured Fe²⁺-TPTZ complex. In FRAP assay, RHE demonstrated a Trolox equivalent antioxidant capacity of 394.7 ± 17.3 mM TE/g dry extract (Table 3). The different antioxidant results obtained from the three assays may reflect differences in the capacity of compounds in the extract to quench DPPH and ABTS free radicals and to reduce ferric ion *in vitro*. Among the methods used, ABTS and FRAP assays are the most correlated, a finding that was formerly reported^{68,69}. It should be noted that the antioxidant assays are preferably performed in the context of the whole organism to obtain more reliable information⁷⁰, which is complemented in the present work by *in vivo* biochemical analysis.

In vitro anti-aging potential. Collagen, elastin, and hyaluronic acid represent the major structural components of the dermal extracellular matrix (ECM). Making up 80% of the skin dry weight, collagen is responsible for the skin tensile strength⁷¹. Brittle when dry but flexible and elastic when moist, elastin fibres maintain skin elasticity⁷². In addition, the mucopolysaccharide hyaluronic acid supports skin viscoelasticity, smoothness, and hydration⁷³. Extrinsic skin aging is mainly attributed to the repeated exposure to solar UV radiation (photoaging), which causes overproduction of reactive oxygen species (ROS), leading to physical changes in the ECM. ROS are known to induce the expression of proteolytic enzymes, such as matrix metalloproteinases (MMPs), e.g., collagenase; serine proteases, e.g., elastase; as well as the glycosidase enzyme hyaluronidase^{74–76}. These are key enzymes in the skin aging process, responsible for the degradation of collagen, elastin, and hyaluronic acid leading to remodelling of ECM and loss of skin elasticity.

To furnish preliminary insights regarding its anti-aging potential, rosemary extract was assessed for its *in vitro* anti-elastase, anti-collagenase, and anti-hyaluronidase activities. RHE demonstrated good dose-dependent inhibition of elastase activity with IC₅₀ value of 57.6 µg/mL close to the reference standard 1,10-phenanthroline (IC₅₀ = 25.6 µg/mL). The extract showed mild anti-collagenase and anti-hyaluronidase effects (IC₅₀ of 520.2 µg/mL and 448.1 µg/mL, respectively) (Table 4).

Interestingly, elastase enzyme has been reported to activate MMP precursors leading to further degradation of ECM⁷⁷. Additionally, elastase was found to degrade decorin, a proteoglycan that binds to and protects collagen fibrils from cleavage by MMP. This renders collagen more susceptible to the proteolytic action of MMP³⁵. Inhibition of elastase can hence stop subsequent degradation steps. Pentacyclic triterpenoids, e.g. lupeol and ursolic acid, are known to inhibit elastase⁷⁸. Since collagenase is a zinc-containing enzyme, phenolic compounds,

Sample	IC ₅₀ (µg/mL)		
	Elastase	Collagenase	Hyaluronidase
RHE	57.61 ± 2.93	520.2 ± 26.5	448.1 ± 22.8
1,10-Phenanthroline	25.6 ± 1.3	340.8 ± 17.3	234.6 ± 11.9

Table 4. *In-vitro* antiaging potential of *R. officinalis* hexane extract.

e.g. flavonoids, phenolic acids, phenolic diterpenes, tannins, and tocopherols (known as metal chelators), were reported to inhibit this metalloproteinase⁷⁹.

In vitro wound healing potential. Wound healing includes the formation and remodelling of new tissues. Migration and proliferation of cells at the wound edge are necessary to close the wound and repair the injured tissue. Many plants have been used in folk medicine to accelerate this process and to prevent infection, such as calendula, for which the wound healing potential was established clinically⁸⁰. In a wound-healing scratch assay, RHE improved the migration and repopulation of keratinocytes at the scratched area and considerably narrowed the scratched gap relative to the control. At 10 µg/mL, RHE showed a closure percentage of 91.85 ± 5.1%, compared to 59.25 ± 3.3 of the control; results superior to calendula hexane and ethanol extracts⁸¹.

Cytotoxic activity. Natural anti-aging interventions include the use of medicinal and aromatic plants known to contain bioactive phytochemicals exerting a myriad of pharmacological activities. Foremost is the issue of safety. The chemical composition of certain plant extract can change according to its geographical origin, growing and processing conditions, solvent used as well as the extraction method. Safety assessment of natural products should be extract-specific to better identify their biological prospect. Several rosemary extracts and isolated phytoconstituents demonstrated cytotoxic and anticancer effects against cancer cell lines^{22,82–85}. However, little is known about the potential cytotoxic effects of rosemary on normal human cells. RHE revealed very weak cytotoxic effect against normal lung fibroblast WI38 cell line (IC₅₀ of 1227.7 ± 14.3 µg/mL) compared with acyclovir (IC₅₀ = 48.65 ± 3.2 µg/mL). The extract can be considered relatively safe for use.

In silico molecular docking study. To rationalize elastase inhibition on a structural level, in silico docking study of the nine major constituents of RHE, as indicated by GCMS analysis, was performed revealing that two components, verbenone and α-amyrin, were able to bind effectively to elastase active site better than the control 1,10-phenanthroline with a Glide G-score of −5.327 and −4.563 kcal/mol, respectively, compared to −4.556 kcal/mol for 1,10-phenanthroline (Table 5). The superior score, especially for verbenone, explains the good inhibitory effect of RHE against elastase enzyme in vitro. Indeed, verbenone was previously reported as potent inhibitor of elastase enzyme with IC₅₀ in the picomolar range⁸⁶. The remaining 7 constituents showed docking scores lower than the control and were therefore excluded as being solely responsible for the in vitro anti-elastase activity of RHE.

The docking pose of verbenone in elastase revealed the formation of a major hydrogen bond with the backbone amide nitrogen of Val224 through its carbonyl group (Fig. 1A,B). This critical interaction plays a major role in the anchorage of verbenone to the binding site of the enzyme. The rest of the small hydrophobic skeleton then buries itself in the binding site groove forming Van der Waal interactions with the hydrophobic side chains of surrounding residues, with minimal exposure to the aqueous medium. Due to verbenone small size and the presence of a hydrogen bond donor, it can fit easily in elastase active site and form non-covalent interactions that promote enzyme inhibition.

In contrast, the docking poses of verbenone in collagenase and hyaluronidase binding sites are unfavourable. In collagenase, verbenone formed two hydrogen bonds with the backbone nitrogen of Leu185 and Ala186, along with Van der Waal interactions with nearby hydrophobic residues, e.g., Leu185 and Tyr244. However, verbenone failed to interact with the active site zinc, which is crucial for collagenase inhibition. Due to this lack of ligand–metal coordination, verbenone failed to inhibit collagenase enzyme (Fig. 1C,D).

In hyaluronidase binding site, verbenone formed a hydrogen bond to the side chain hydroxyl group of Ser303 (Fig. 1E,F which constitutes an important residue in the binding of hyaluronic acid to hyaluronidase as shown in the co-crystal structure (PDB ID: 1FCV). Furthermore, per-residue interaction scores showed that the hydrogen bond strength of verbenone to Ser303 in hyaluronidase (−0.320 kcal/mol) is greater than hydrogen bond strength of verbenone to Val224 in elastase (−0.286 kcal/mol). However, the overall binding pose of verbenone to hyaluronidase does not qualify it to become an inhibitor due to the superficial binding of verbenone to the active site of hyaluronidase, prohibiting the ligand from immersing itself in the folds of the active site and escaping the aqueous medium. The over-exposure of the hydrophobic skeleton of verbenone to the aqueous medium has made the overall binding of the ligand unstable, and therefore its activity minimal.

It is noteworthy that in collagenase and hyaluronidase docking experiments, the control 1,10-phenanthroline scored higher than RHE major constituents (Table 5), among which camphor showed the best score and binding pose. The docking experiment of camphor in collagenase binding site showed better binding compared to verbenone. Camphor directed its carbonyl oxygen towards the active site zinc and approached it at 1.98 Å. At this distance, the carbonyl could form a mono-dentate metal chelation interaction with the active site zinc (Fig. 2A,B). Furthermore, the hydrophobic skeleton of camphor was buried among the hydrophobic residues Pro242, Ile243, Leu185, Tyr244, and Tyr214. Despite the good binding pose of camphor in the binding site of collagenase, the

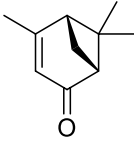
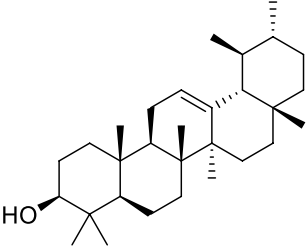
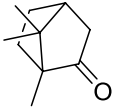
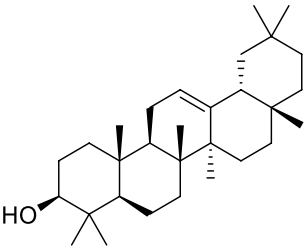
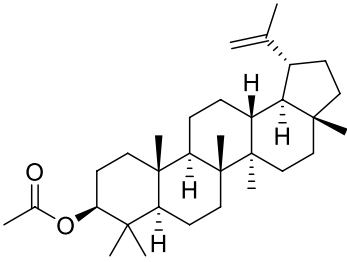
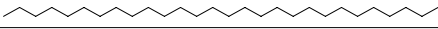
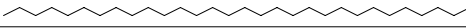
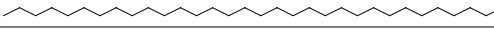

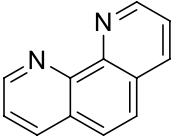
Compound	Compound structure	Glide G-score		
		Elastase	Collagenase	Hyaluronidase
Verbenone		-5.327	-5.281	-3.829
α -Amyrin		-4.563	-3.508	-3.398
Camphor		-4.273	-5.402	-4.515
β -Amyrin		-3.515	-3.765	-3.339
Lupeol acetate		-3.267	-3.465	-2.072
Octacosane		-2.424	-3.903	-0.698
Triacontane*		*	-2.95	-0.885
Doctriacontane*		*	-4.767	-0.775
Tetratriacontane*		*	*	*
1,10-Phenanthroline		-4.556	-6.931	-4.714

Table 5. Docking scores of RHE major constituents against elastase, hyaluronidase and collagenase as compared to the control, 1,10-phenanthroline. *Compounds were rejected by the docking engine due to their exceedingly large size.

expected activity of camphor against collagenase may not be ideal due to the lack of another metal chelation interaction with zinc, since a bi-dentate metal coordination is required for potent collagenase inhibition.

In case of hyaluronidase, camphor formed of hydrogen bonds. The carbonyl oxygen of camphor bonded to the hydroxyl side chain of Ser303 and the backbone amide nitrogen of Ser304 (Fig. 2C,D). Nevertheless, camphor binding to hyaluronidase could not be stable due to the exposure of the hydrophobic skeleton of camphor to the aqueous medium. These findings are in agreement with the in vitro anti-aging results. Verbenone, with its higher docking score and binding mode, may be responsible for the overall anti-elastase activity of the extract.

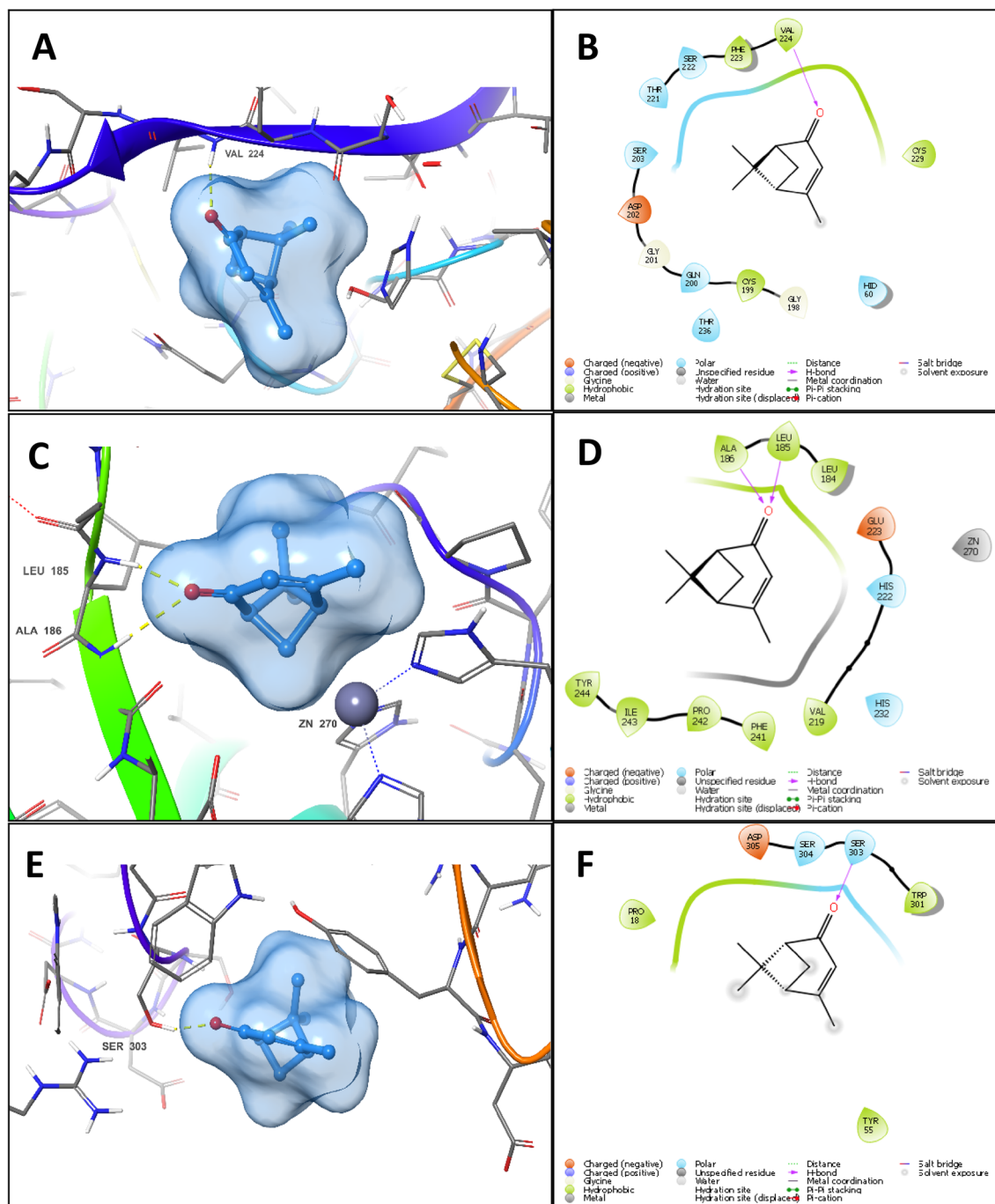


Figure 1. 3D docking pose and 2D interaction diagram of verbenone in the binding site of elastase (A,B), collagenase (C,D) (showing lack of metal coordination interaction) and hyaluronidase (E,F) (showing excessive water exposure).

Meanwhile, the docking poses of camphor and verbenone against collagenase and hyaluronidase revealed that these compounds could not inhibit both enzymes, a result that validates our experimental findings.

Characterization of LNC. The results of the PS distribution and ZP measurements are listed in Table 6. As shown, the PS of blank LNC, 4% RM-LNC (rosemary-loaded lipid nanocapsules), and 10% RM-LNC were 42.28 ± 0.417 nm, 55.20 ± 0.218 nm, and 64.81 ± 1.113 nm, respectively. The obtained PS of blank LNC was comparable to previous results regarding the small size of LNC^{87,88}. As observed, rosemary loading into LNC resulted in a significant ($p < 0.05$) increase in PS of RM-LNC, which may be attributed to the increase in the mass of the oily core with subsequent increase in PS⁸⁹. Both blank and rosemary-loaded LNC showed homogenous PS distribution as reflected by the low PDI values (< 0.3). Despite rosemary loading into LNC resulted in significant ($p < 0.05$) increase in PDI values, they still reflect the narrow particle distribution.

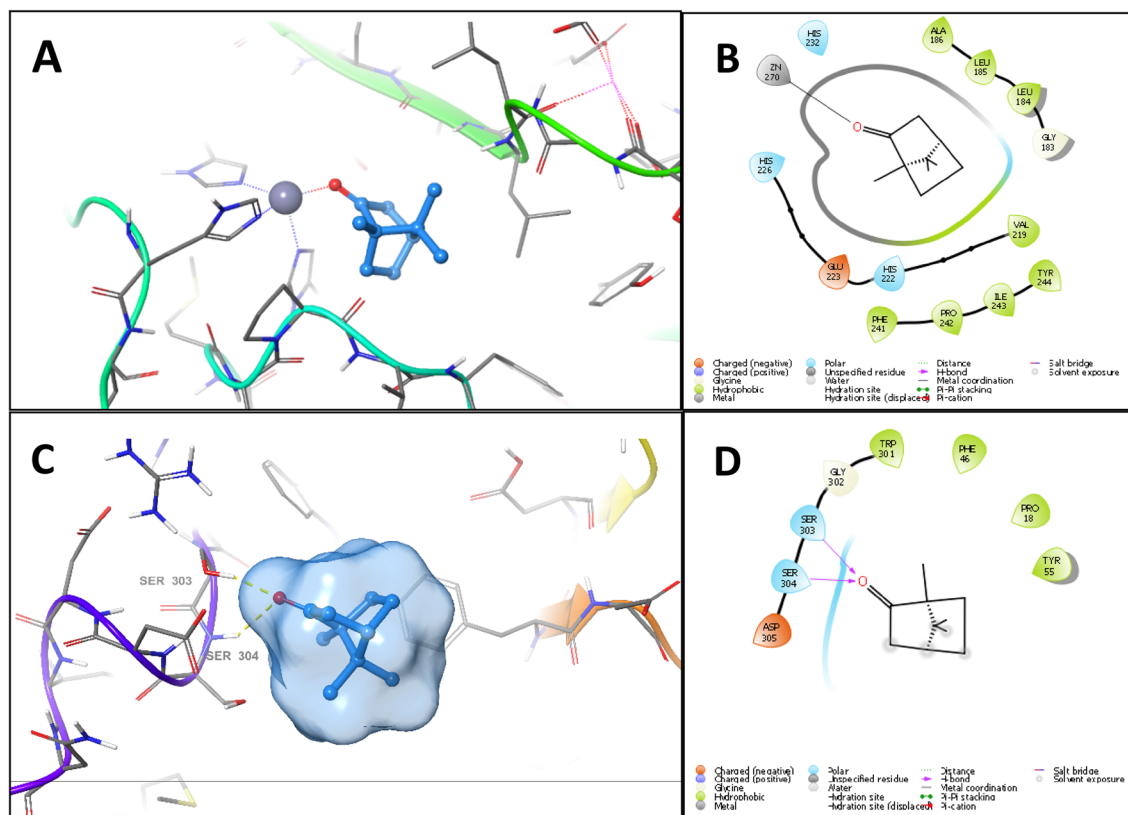


Figure 2. 3D docking pose and 2D interaction diagram of camphor in the binding site of collagenase (A,B) and hyaluronidase (C,D).

Formula	Particle size (nm) \pm S.D	PDI \pm S.D	Zeta potential (mV) \pm S.D
Blank LNC	42.28 \pm 0.417	0.048 \pm 0.001	-12.6 \pm 1.41
Blank LNC gel	45.72 \pm 0.079	0.032 \pm 0.004	-11.2 \pm 0.70
4% RM-LNC	55.20 \pm 0.218	0.175 \pm 0.016	-13.1 \pm 0.63
4% RM-LNC gel	56.55 \pm 0.384	0.207 \pm 0.014	-13.4 \pm 0.91
10% RM-LNC	64.81 \pm 1.113	0.262 \pm 0.028	-15.4 \pm 2.62
10% RM-LNC gel	66.13 \pm 1.306	0.249 \pm 0.007	-15.6 \pm 0.89

Table 6. Composition and characterization of blank and rosemary-loaded lipid nanocapsules (RM-LNC). PDI: polydispersity index, S.D.: standard deviation.

The small PS associated with homogenous distribution is a main characteristic of LNC, which favours its application in topical use. Small PS represents a main advantage due to the increased surface area of the particles forming a dense monolayer and promoting better skin contact, which is needed to achieve high protection against UV radiation⁹⁰. Moreover, previous studies reported the enhanced penetration of the lipid nanocarriers into the epidermal layer as the PS decreases^{87,91,92}.

The ZP values of blank LNC, 4% RM-LNC, and 10% RM-LNC were -12.6 ± 1.41 mV, -13.1 ± 0.63 mV, and -15.4 ± 2.62 mV, respectively. The negative charge of the prepared LNC is attributed to the existence of negatively charged phospholipids and the PEG dipoles that took part in the formation of the LNC shell^{93–95}. It has been reported that colloidal stability increases as the ZP values increase ($\geq \pm 30$ mV), which is attributed to the electric repulsion between particles. However, the stability of LNC with low ZP values is attributed to steric stabilization of LNC by their tensioactive rigid membrane^{33,34}. It can be observed that rosemary-loaded LNC displayed higher negative value of the ZP than blank LNC. A clear explanation was provided by a previous study conducted by Valcourt et al. 2016, which stated that the incorporation of oils into the lipid core of the LNC had a negative impact on the density of PEGylated surfactant at the particle surface with a subsequent increase in the contact area between the lipid molecules and the external phase and resulted in an increase in the absolute value of the ZP⁸⁹.

Group	Antioxidant parameters			Anti-inflammatory parameters			Anti-wrinkling parameters			
	Catalase	SOD	GSH	IL-6	IL-1 beta	NF-KB	GM-CSF	MMP1	Elastase	Neprilysin
	U/g tissue	U/g tissue	Pg/g tissue	Pg/g tissue	Pg/g tissue	ng/g tissue	Pg/g tissue	ng/g tissue	ng/g tissue	Pg/g issue
NC	38.7 ± 1.14	45.6 ± 1.29	50.6 ± 1.10	14.1 ± 1.18	20.4 ± 1.2	23.4 ± 1.19	6.4 ± 0.87	2.1 ± 0.68	1.6 ± 0.85	26.7 ± 1.68
PC	7.8 ± 0.95*	12.3 ± 1.54*	17.4 ± 1.13*	40.1 ± 1.85*	46.1 ± 0.84*	55.2 ± 0.75*	29.1 ± 1.25*	9.5 ± 1.06*	7.9 ± 1.05*	51.2 ± 1.15*
T1	14.3 ± 0.92* [ⓔ]	19.7 ± 0.65* [ⓔ]	24.5 ± 1.22* [ⓔ]	27.6 ± 1.65* [ⓔ]	19.1 ± 1.35* [ⓔ]	36.5 ± 1.16* [ⓔ]	19.1 ± 1.35* [ⓔ]	6.7 ± 0.85* [ⓔ]	5.6 ± 0.79* [ⓔ]	40.1 ± 1.12* [ⓔ]
T2	29.5 ± 1.35* ^{ⓔ#}	24.8 ± 0.98* ^{ⓔ#}	29.5 ± 1.35* ^{ⓔ#}	23.4 ± 1.42* ^{ⓔ#}	29.7 ± 1.3* ^{ⓔ#}	32.4 ± 1.18* ^{ⓔ#}	15.7 ± 1.2* ^{ⓔ#}	5.4 ± 0.98* ^{ⓔ#}	4.6 ± 1.02* ^{ⓔ#}	35.2 ± 1.4* ^{ⓔ#}
T3	38.2 ± 1.64* ^{ⓔ#a}	32.9 ± 0.88* ^{ⓔ#a}	38.2 ± 1.64* ^{ⓔ#a}	16.9 ± 1.85* ^{ⓔ#a}	23.1 ± 1.06* ^{ⓔ#a}	25.4 ± 1.06* ^{ⓔ#a}	9.2 ± 1.05* ^{ⓔ#a}	3.2 ± 0.56* ^{ⓔ#a}	2.3 ± 0.65* ^{ⓔ#a}	28.9 ± 1.8* ^{ⓔ#a}
T4	12.3 ± 0.65* ^{ⓔ#+++}	15.8 ± 1.05* ^{ⓔ#+++}	20.4 ± 1.16* ^{ⓔ#+++}	32.1 ± 1.88* ^{ⓔ#+++}	23.7 ± 1.23* ^{ⓔ#+++}	40.3 ± 1.06* ^{ⓔ#+++}	23.7 ± 1.23* ^{ⓔ#+++}	7.7 ± 0.62* ^{ⓔ#+++}	6.4 ± 0.56* ^{ⓔ#+++}	44.6 ± 1.65* ^{ⓔ#+++}

Table 7. Effect of UVB-irradiation and different formulations on the oxidative stress, inflammatory and wrinkling markers in rats. NC: Negative control (normal rats), PC: positive control (subjected to UVB irradiation and received no treatment), while T1, T2, T3 and T4 received RHE, 4%-RM-LNC gel, 10% RM-LNC gel and plain LNC gel. Each value is presented as mean ± standard error of the mean (SE) for 10 rats. *Statistically significantly different from the normal control group ($P < 0.05$). [ⓔ]Statistically significantly different from the positive control group ($P < 0.05$). [#]Statistically significantly different from the T1 group ($P < 0.05$). ^aStatistically significantly different from the T2 group ($P < 0.05$). ⁺⁺⁺Statistically significantly different from the T3 group ($P < 0.05$).

Characteristics of RM-LNC gels. Incorporation of lipid nanocarriers into mucoadhesive gels combined the advantages of a topically delivered formulation with those of nanocarriers in the same final product. These advantages include ease of application, high mucoadhesion with extended skin contact, and slow drug release rate^{96,97}.

Based on our previous study, 3% w/w HEC had a viscosity of 30 to 40 poise⁹⁸, which is considered acceptable viscosity for sunscreen gels as reported in previous study⁹⁹. Therefore, 3%w/w HEC was chosen to be added to the LNC dispersion. It was expected that the presence of LNC might have an influence on the measured viscosity of the gel; therefore, the rheological properties of the RM-LNC gels were investigated. In addition, RM-LNC gel was characterized in terms of PS, PDI, and ZP.

Blank LNC, 4%RM-LNC, and 10%RM-LNC gels showed PS equals 45.72 ± 0.079 nm, 56.55 ± 0.384, nm and 66.13 ± 1.306 nm, respectively, where no significant ($p > 0.05$) increase in PS was reported upon LNC incorporation into HEC gel. As observed, all LNC gels are characterized by low PDI values and negatively charged ZP, which indicates their physical stability upon addition of the gelling agent.

The respective viscosity of blank LNC, 4%RM-LNC, and 10%RM-LNC gels were 32.91 ± 1.54, 35.42 ± 3.89, and 39.55 ± 2.76 poise, respectively, which are acceptable values for the topical application. The pH values of blank LNC, 4%RM-LNC, and 10%RM-LNC gels were in the range of 6–8, which are considered safe for application as a sunscreen for its photoprotective effect.

In vivo studies. *Biochemical analysis.* Unprotected exposure to UVB irradiation results in skin damage; this can be assessed by the validation of different biochemical markers. In this study, the suggested protective effect of the prepared RM-LNC in comparison to RHE was investigated by measuring the level of some antioxidant, anti-inflammatory, and anti-wrinkling markers.

Antioxidant markers. The non-enzymatic antioxidants, GSH, as well as the antioxidant enzymes, SOD and CAT, were measured in the different studied groups. It is expected that the level of these enzymes decreases in oxidative stress conditions, like exposure to UV irradiation. As listed in Table 7, the marked decrease in their level in case of the positive control group compared to the negative one ($p < 0.05$) was abolished in the groups administered with the RHE as well as the RM-LNC gels, suggesting that rosemary can replenish antioxidants. This validates the initial in vitro screening, sheds light on skin penetration of applied formulae, and confirms their effectiveness in biological systems. The more potent effect of RM-LNC gels compared to the RHE ($p < 0.05$) is expected based on the above discussed in vitro study as well as the visual examination of the dorsal rats' skin before sacrificing. The enhanced RHE solubilization and release, reduced PS, as well as the elastic properties of the designed LNC can assure an enhanced skin penetration and photoprotective effect. Some previous studies have reported that the PS range recorded for prepared formulae facilitates drug penetration and accumulation into the skin, which allows a localized and site-specific drug effect^{87,100}.

Anti-inflammatory activity. UVB exposure up-regulates inflammatory cytokines causing skin damage¹⁰¹. The values seen in Table 7 show that UVB exposure induced a significant increase in the inflammatory markers (IL-1 β , IL-6, and NF-kB) of the positive control group compared to those of the negative control ($p < 0.05$). This effect decreased in case of the groups pre-treated with RHE and RM-LNC ($p < 0.05$). However, the effect of the RM-LNC formulae was higher than the RHE ($p < 0.05$). As discussed above, the superior effect of the RM-LNC against the inflammatory reactions induced by UVB irradiation can be due to the intrinsic properties of the designed LNC, which can breach the skin barrier and penetrate deeply into the inner skin layers. This reduction in photo-inflammation was evidenced by decreased erythema, edema, and skin thickness. The observed anti-inflammatory effect can be attributed to the rich triterpenoids and phenolic diterpenes content of rosemary.

Rat	Negative control		Positive control		T1		T2		T3		T4	
	Er	Ed	Er	Ed	Er	Ed	Er	Ed	Er	Ed	Er	Ed
1	1	0	4	3	1	0	1	0	2	0	1	0
2	0	0	3	4	1	0	1	0	1	1	2	1
3	0	0	4	4	1	0	0	0	2	1	2	1
4	1	0	4	3	2	1	0	1	2	0	2	1
5	1	0	4	4	2	1	1	0	1	1	2	1
6	1	0	4	4	1	1	1	0	1	1	1	0
Average	0.66	0	3.83	3.66	1.33	0.5	0.66	0.166	1.5	0.66	1.66	0.66
PII	0.66	±0.15	7.5 ⁺⁺⁺	±0.16	1.83 ^{†a}	±0.12	0.83 ^{†a}	±0.13	2.16 ^{†a}	±0.14	2.33 ^{†a}	±0.16

Table 8. Cutaneous irritancy test. ⁺⁺⁺Significant ($p < 0.001$) when compared to group 1. ^aSignificant ($p < 0.001$) when compared to group 2. [†]Non-significant ($p > 0.05$) when compared to group 1.

The major components of RHE, α - and β -amyryn, were reported to exert anti-inflammatory activity through the activation of the cannabinoid receptors¹⁰². Carnosic acid, carnosol and rosmanol suppress nitric oxide and TNF- α , downregulate COX2 expression and inhibit PGE2 synthase-1, iNOS and 5-lipoxygenase^{103–105}. Moreover, the anti-inflammatory activity of the monoterpenoid eucalyptol was well established through the suppression of lipopolysaccharide-induced pro-inflammatory cytokines, e.g. IL-1 β , IL-6, and NF- κ B²¹. In addition, the synergism with other existing phytoconstituents cannot be precluded.

Anti-wrinkling markers. Exposure to UVB irradiation triggers the production of free radicals, which upregulate the production of matrix metalloproteinases (MMPs). Degradation of the collagen and elastin network is caused by MMPs¹⁰⁶, leading to skin wrinkling. UVB irradiation causes keratinocytes to secrete IL-1, which stimulates GM-CSF secretion and triggers fibroblasts to stimulate their expression of neprilysin/NEP, which results in the deterioration of the three-dimensional fibre networks and the loss of skin elasticity and wrinkles formation^{107,108}. As observed in Table 7, the levels of MMP1, GM-CSF, neprilysin, and elastase are higher in the positive control group than in the negative control one ($p < 0.05$). Application of RHE or RM-LNC protected the skin from wrinkling and aging ($p < 0.05$). As expected, the photoprotective effect of the studied formulae was significantly superior ($p < 0.05$). Surprisingly, the major ingredient in RHE, α -amyryn, did not provide in vitro protection against UVB damage in earlier reports⁴³, suggesting that the observed photoprotection can be mediated by potentiating interactions among several constituents, including the minor ones.

Cutaneous irritancy test. Skin applied formulae are required to be innocuous, neither creating irritancy nor allergenicity¹⁰⁹. Both the plain and rosemary-loaded LNC gels were tested to evaluate the safety of each component of the preparations. The results shown in Table 8 proved the non-irritancy of tested gels (PII < 2) all over the period of the experiment (72 h). Statistical analysis shows that the formalin solution (group 2) was significantly irritant ($p < 0.001$) compared to the control group (group 1) and all the gels, whereas there was no significant difference ($p > 0.05$) between all gels and the control group.

Histopathological examination. The photos of the skin subjected to histopathological study are displayed in Fig. 3. The negative control group demonstrated normal morphological features of skin layers including thin intact epidermal layer with well-organized apparent intact subcellular details of different keratinocytes in different zones, intact dermal layer with abundant collagen fibres, minimal inflammatory cells infiltrates, and normal vasculatures. On the other hand, the positive control group revealed significant increase of epidermal thickness with alternated areas of apparent intact or pyknotic basal cells layer accompanied with mild to moderate dermal mononuclear inflammatory cells infiltrates as well as congested subepidermal blood vessels and focal hemorrhagic zones. A certain improvement of the condition can be observed in rats treated with RHE; however, samples revealed moderate reduction of epidermal thickening with persistence of degenerative changes records of basal cell layer, mild subepidermal mononuclear cells infiltrates, and congested blood vessels.

Group T2 samples showed moderate reduction of epidermal thickening as shown in Fig. 3, with persistence of degenerative changes records of basal cell layer and mild subepidermal mononuclear cells infiltrates. However, normal subepidermal vasculatures were recorded.

Group T3 samples demonstrated almost intact well-organized skin layers with minimal records of abnormal morphological features all over epidermal and dermal layers.

Finally, group T4 showed abundant records of degenerated and pyknotic epidermal keratinocytes with normal epidermal thickness ranges accompanied with mild occasional sub-epidermal inflammatory cells infiltrates as well as congested BVs.

Previous studies have established the anti-inflammatory and photoprotective activities of rosemary polyphenols and polar extracts^{19,110}. However, this is the first report of the photoprotective potential of rosemary hexane extract which is often regarded as agro-industrial processing waste during the extraction of polyphenols.

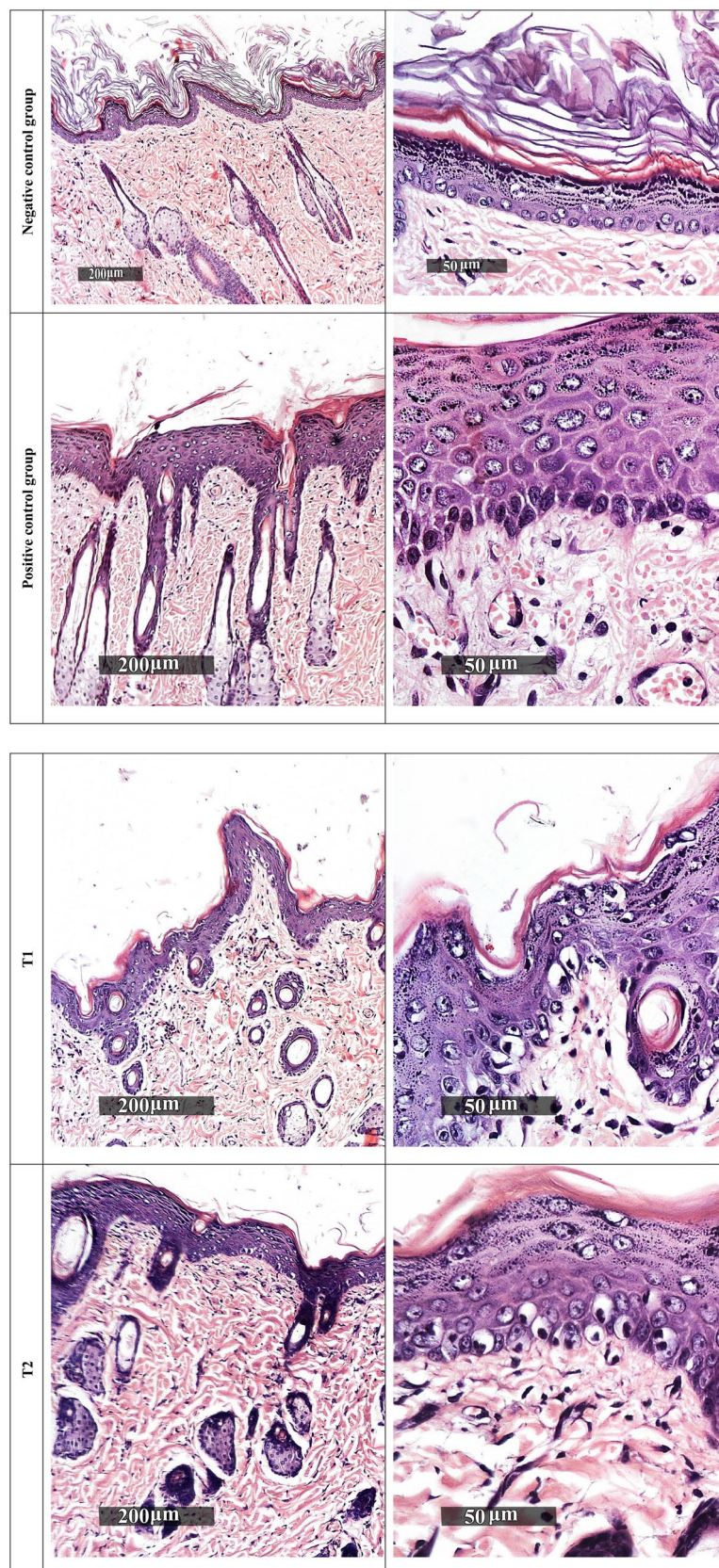


Figure 3. Histopathological examination of rat dorsal skin. Negative control: normal rats, positive control: subjected to UVB irradiation and received no treatment, while T1, T2, T3 and T4 received RHE, 4%-RM-LNC gel, 10% RM-LNC gel and plain LNC gel.

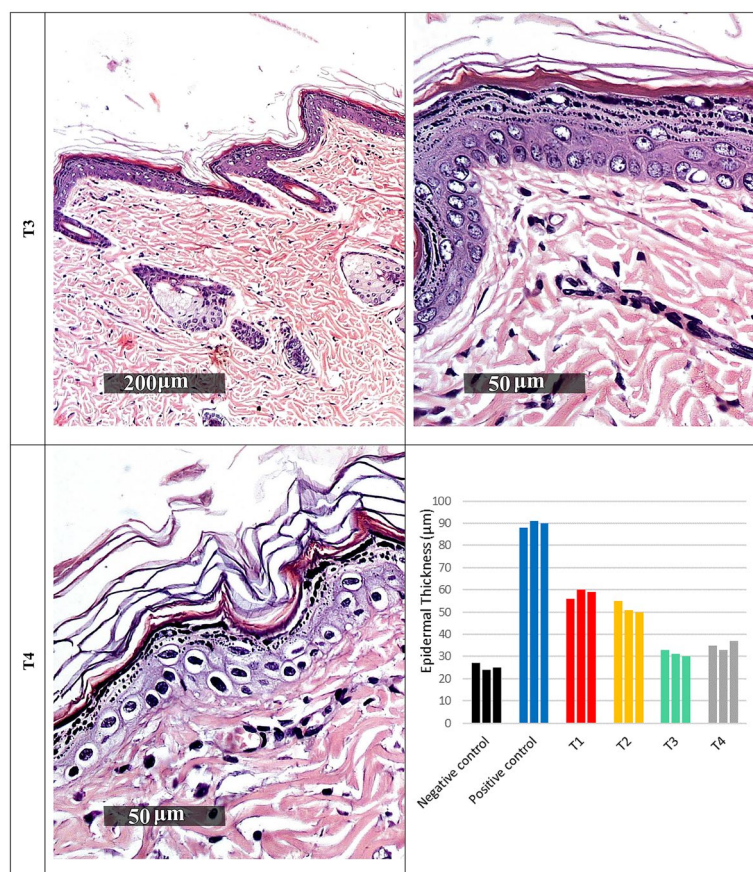


Figure 3. (continued)

Materials and methods

Materials. Kolliphor® HS 15 (Solutol® HS 15), a mixture of free polyethylene glycol 660 and polyethylene glycol 660 hydroxy stearate) was purchased from Sigma-Aldrich, Zwijndrecht, Netherlands. Labrafac lipophile WL1394 (triglyceride medium chain, caprylic/capric TG) and soybean phosphatidylcholine (Epikuron™170 (EP) were a kind gift from Gattefosse, Saint-Priest, France. Sodium chloride, methanol, and n-hexane were purchased from Adwic, El-Nasr Pharmaceutical Co., Cairo, Egypt. Hydroxyethyl cellulose (HEC) (2% solution has a viscosity of 640.9 cP) was kindly supplied by Memphis Co., Cairo, Egypt.

Plant material and extraction. Leaves from three nearby shrubs of *Rosmarinus officinalis* L. were collected at the Medicinal Plants Station, Faculty of Pharmacy, Ain Shams University (Cairo) in July 2019 and were kindly authenticated by Mrs. Therese Labib, plant taxonomist at the Ministry of Agriculture. Experimental research on plant, including the collection of plant material, complied with relevant institutional, national, and international guidelines and legislation. The study did not include any species at risk of extinction or endangered species. A voucher specimen was deposited at the herbarium of Pharmacognosy Department, Faculty of Pharmacy, Ain Shams University (Cairo) for referencing (PHG-P-RO-328). Fresh leaves were ground in a kitchen-type milling machine and macerated in distilled n-hexane (2 × 3 L) for 48 h. Extraction was assisted by sonication for three intervals 10 min each. After filtration, the extract was evaporated under reduced pressure at 40 °C using a rotary-type evaporator (Büchi, Switzerland) to yield a green greasy solid residue (2.1% w/w) which was stored at –20 °C until needed.

GC-MS analysis. A Shimadzu GC-MS-QP2010 was used to perform the GC-MS analyses (Shimadzu Corporation, Kyoto, Japan) as recently reported¹¹¹.

LC-ESI-HRMS analysis. For the chromatographic separation, 6530 Q-TOF LC/MS (Agilent Technologies) equipped with an autosampler (G7129A), a Quaternary Pump (G7104C), and a Column Compartment (G7116A) was used. The injection volume was 5 μL. The analytes were separated on a Zorbax RP-18 column (150 mm × 3 mm, 2.7 μm) in a flow rate of 0.3 mL/min. The mobile phase was composed of solvent A (aqueous formic acid, 0.1% v/v) and solvent B (0.1% formic acid/acetonitrile). A gradient mode was implemented as follows; at t = 0–2 min, solvent A/solvent B (90/10); at t = 10 min, solvent A/solvent B, (80/20); at t = 52–80 min, 100% solvent B. Mass spectra were acquired using ESI in negative ionization mode with a capillary voltage of 4500 V. The mass spectra were recorded in the *m/z* range of 50–3000 *m/z*. The gas temperature and drying gas flow rate were 200 °C and 8 L/min, respectively. The skimmer and fragmentation voltages were set at 65 and

130 V, respectively, and collision energy was 10 V. The nebulization pressure was 58 psi. Data processing was performed using MassHunter workstation B.06.00 (Agilent Technologies, 2012) and compounds were tentatively identified according to their mass spectra, accurate mass and retention time, in comparison with literature.

In vitro antioxidant activity. *DPPH radical scavenging activity.* The scavenging activity of the stable 2,2-diphenyl-1-picrylhydrazyl (DPPH) free radical by RHE was assessed according to the method reported by Boly et al.¹¹².

ABTS radical scavenging assay. This assay was carried out according to the method previously reported by Arnao et al.¹¹³.

FRAP assay. The method is based on the reduction of a ferric-tripyridyltriazine (Fe³⁺-TPTZ) complex to its intensely blue ferrous form, at low pH, as previously described¹¹⁴.

In vitro anti-aging potential. *Anti-elastase assay.* The elastase inhibitory activity was assessed fluorimetrically using the EnzCheck® elastase assay kit (Molecular Probes, Laiden, Netherlands). A 1 mg/mL stock solution of the substrate (DQ elastin) was prepared in deionized water. Porcine pancreatic elastase stock solution was prepared in deionized water at 100 U/mL and dilutions were made in Tris–HCL buffer. Pre-incubation of 50 µL of different dilutions of the extract (inhibitor) with 100 µL of the enzyme was done for 15 min followed by the addition of the substrate (50 µL). Controls were prepared with buffer instead of extract. Fluorescence intensity was continuously measured for 20 min in a fluorescence microplate reader equipped with standard fluorescein filters (λ_{ex} 505 nm, λ_{em} 515 nm). Subtraction of background fluorescence was done in no-enzyme wells. 1,10-Phenanthroline was used as a standard elastase inhibitor. The IC₅₀ is the concentration of the extract required to inhibit 50% of elastase activity.

$$\text{The percentage of elastase inhibition (\%)} = (1 - S/C) \times 100$$

where S is the corrected fluorescence of the extract samples and C is the corrected fluorescence of the control.

Anti-collagenase assay. The evaluation of collagenase inhibitory activity was performed fluorimetrically in a microplate reader. Briefly, the self-quenched BODIPY conjugate of gelatin (Type B) was used as a fluorogenic substrate to monitor the activity of collagenase (Biovision, CA, USA). Collagenase stock solution was prepared in 50 mM Tricine buffer at 0.8 U/mL and the substrate (BODIPY) was dissolved in Tricine buffer to 2 mM. One microliter of different concentrations of the extract (1, 10, 100, and 1000 µg/mL) was incubated with the 5 µL collagenase in buffer and 44 µL Tricine buffer for 15 min before adding the substrate. (1, 10)-Phenanthroline was used as a positive control. The reaction is initiated by mixing two µL of the substrate with the previous reaction mixture. Negative controls were prepared with the buffer. Fluorescence intensity was monitored (λ_{ex} 490 nm, λ_{em} 520 nm, 515 nm cut-off) in a kinetic mode at 37 °C for 30–60 min.

$$\text{The percentage of collagenase inhibition (\%)} = (1 - S/C) \times 100$$

where S is the corrected fluorescence of the extract sample and C is the corrected fluorescence of the control.

Anti-hyaluronidase assay. A turbidimetric assay was performed to assess the hyaluronidase inhibitory activity using QuantiChrom™ Hyaluronidase Inhibitor Screening Assay Kit (BioAssay Systems, CA, USA). Bovine hyaluronidase (type-1-S, Sigma Aldrich, St. Louis, MO, USA) was diluted to 10 U/mL in buffer. From this solution, 40 µL were transferred to a 96-well plate. Instead, enzyme buffer (40 µL) was used for No Enzyme Control (NEC), while hyaluronidase (40 µL) was used for No Inhibitor Control (NIC). To the NIC and NEC wells, 20 µL DMSO were added and to the sample wells 20 µL of the desired extract concentrations were added followed by incubation for 15 min at room temperature. The substrate (40 µL) was added and the plate was incubated for 20 min. The stop reagent (160 µL) was used to halt the enzymatic reaction and forms turbidity with any residual hyaluronic acid. Plate was incubated for 10 min and the optical density was read at 600 nm. The percentage inhibition was calculated as follows:

$$\% \text{ Inhibition} = 1 - [(OD_{\text{NEC}} - OD_{\text{sample}})/(OD_{\text{NEC}} - OD_{\text{NIC}})] \times 100$$

where OD_{NEC}, OD_{NIC}, and OD_{sample} represent the optical density values of the No Enzyme Control, No Inhibitor Control, and the extract.

Scratch-wound healing assay. Effect of RHE on keratinocytes migration was evaluated using the scratch assay as previously described¹¹⁵.

Cytotoxicity assay. The cytotoxicity of RHE extract was evaluated against human normal lung fibroblasts cell line WI-38 using MTT (3-(4,5-dimethylthiazol-2-yl)2,5-diphenyl tetrazolium bromide) assay¹¹⁶ as recently described¹¹¹.

In silico molecular modelling. All docking experiments were done using Glide docking engine (Schrödinger Release 2020–4: Glide, Schrödinger, LLC, NY, 2020). The crystal structures of the three target enzymes, elastase (PDB ID: 1ELC, 1.75 Å), collagenase (PDB ID: 2D1N, 2.37 Å), and hyaluronidase (PDB ID:

1FCV, 2.65 Å), were downloaded from the Protein Data Bank (PDB). The crystal structures were co-crystallized with non-covalent inhibitors. The PDB files were imported into Maestro and prepared using the protein preparation wizard and standard protein preparation protocol. The docking grid was then generated using the grid receptor grid generation module and the co-crystallized ligand was selected as the grid centre. The ligands were then imported and prepared using Ligprep module and standard ligand preparation protocol. Molecular docking was carried out using Glide Standard Precision and no constraints. Per-residue interaction scores were calculated for selected ligands and residues during docking re-runs using the same procedures.

Preparation of blank and rosemary-loaded LNC. Blank LNC were prepared using the phase inversion method with three temperature cycles⁸⁷. In brief, aqueous phase composed of Solutol® HS 15 (1 g), sodium chloride (0.1 g), and demineralized water (3 g) was mixed with the oily phase of Labrafac (0.9 g) and EP (0.1 g) in a closed container under magnetic stirring for 10 min. The mixture was heated up to 85 °C under magnetic stirring, followed by cooling to 55 °C to ensure phase inversion from w/o emulsion to o/w emulsion. The heating/cooling cycle was repeated two times followed by the addition of 5 ml of cold water (0–2 °C) with magnetic stirring. The LNC dispersions obtained were kept at 4 °C for further investigation. Rosemary-loaded LNC (RM-LNC) were prepared using the same procedure, where the rosemary extract (4%w/w or 10%w/w) was dissolved in the oily phase by magnetic stirring before mixing with the aqueous phase, then the procedure was completed as previous.

Particle size distribution and zeta potential measurements of the prepared LNC. The particle size (PS), polydispersity index (PDI), and zeta potential (ZP) for the prepared blank and RM-LNC were determined at 25 °C using a laser diffraction particle size detector (Zetasizer; Malvern Instruments, Malvern, UK) after suitable dilution.

Preparation and characterization of blank and RM-LNC-based gels. Gels based on LNC were prepared by gradual sprinkling of HEC as gelling agent into the LNC dispersions under magnetic stirring until complete hydration. The gel was sonicated for dissipation of entrapped air and stored at 4 °C for further evaluation¹¹⁷.

The PS, PDI, and ZP of blank and RM-LNC-based gels were measured as previously described after suitable dilution with deionized water with magnetic stirring. Viscosity measurements were conducted using viscometer (Brookfield Engineering Laboratories Inc., Model HADV-II, USA) connected to a digital thermostatically controlled circulating water bath (Polyscience, Model 9101, USA) with spindle 52 at a speed of 50 rpm 25 ± 0.1 °C. Equilibration of the sample for 5 min was made following loading of the viscometer. All studies were performed in triplicates and the average was taken¹¹⁸. The pH of 5% w/w dispersions of the gels in water was determined using pH meter.

In vivo study. *Animals.* The experiment was performed on the hairless skin of adult male Wistar rats weighing between 180 and 220 g (6–8 weeks old) obtained from the animal house of the National Research Center, Cairo, Egypt. The animals were housed in plastic cages and kept in a conditioned atmosphere at 22 ± 3 °C and humidity 50–55% with 12 h light/dark cycles. They were fed standard pellet chow (El-Nasr chemical company, Cairo, Egypt) and were permitted free access to water. This study was conducted in accordance with ethical procedures and policies approved by the Institutional Animal Care and Use Committee of Cairo University, Egypt (Ethical Approval Number IACUC-CU-III-F-42–20). The study followed the recommendations in the ARRIVE guidelines.

Experimental design. The dorsal side of the rats was shaved 24 h before the beginning of the experiment. Sixty rats were randomly divided into six groups, each containing 10 animals: a negative control group (C1) was not exposed to irradiation; a positive control group was subjected daily to UVB irradiation for 10 consecutive days and received no treatment. The other four groups named T1, T2, T3, and T4 received RHE, 4%-RM-LNC gel, 10% RM-LNC gel, and plain LNC gel, respectively, daily one hour before the UVB exposure. A UV lighter (peak emission was 302 nm, CL-1000 M, UVP, Upland, CA, USA) was used for UVB irradiation. UVB irradiation doses were 40–80 mJ/cm² (exposure time was 15–30 s) and the lamp was fixed 5 cm above the platform where rats were placed¹¹⁹.

Tissue preparation. At the end of the experiment, rats were anesthetized by ketamine (85 mg/kg, i.p.), euthanized by cervical dislocation, and the treated skin of each rat was dissected out into two halves. The first half of the dorsal skin of rats was preserved in 10% formalin for histopathological examination. The other half of skin samples were homogenized and subjected to biochemical estimation of the antioxidant, anti-inflammatory, and anti-aging activities of the prepared RM-LNC gels in comparison with the RHE.

Biochemical analysis. *Antioxidant activity.* The level of catalase (CAT), reduced glutathione (GSH), and superoxide dismutase (SOD) reactive substances was estimated as reported previously^{120,121} in the homogenate. Catalase (CAT) ELISA Kit was purchased from Hubei, China, Rat Superoxide Dismutase (SOD) ELISA Kit was purchased from MyBioSource, San Diego, US, and Glutathione peroxidase (GSH) was purchased from Shanghai BlueGene Biotech CO., China.

Anti-inflammatory activity. The level of interleukin 1 beta (IL-1 β), interleukin 6 (IL-6), and nuclear factor-kappa B (NF- κ B) was determined using an enzyme-linked immunosorbent assay (ELISA) kit. Rat NF- κ B ELISA

Skin reaction	Score
Erythema formation (Er.)	
None	0
Very slight erythema	1
Well defined erythema	2
Moderate to severe erythema	3
Severe erythema and scar formation	4
Edema formation (Ed.)	
None	0
Very slight edema	1
Slight edema (edges of area well defined by definite raising)	2
Moderate edema (area raised approximately 1 mm.)	3
Severe edema (raised more than 1 mm. and extending beyond area of exposure)	4

Table 9. Evaluation of skin reactions.

Kit and Interleukin 6 (IL-6) were purchased from CUSABIO, Inc., Wuhan, Hubei, China. Rat interleukin 1 beta (IL-1 β), ELISA Kit was purchased from MyBioSource, San Diego, US.

Anti-wrinkling and anti-photoaging activity. The level of matrix metalloproteinase (MMP-1), granulocyte-macrophage colony-stimulating factor (GM-CSF), neprilysin, and elastase enzymes were determined using an enzyme-linked immunosorbent assay (ELISA) kit. Rat Granulocyte-Macrophage Colony Stimulating Factor (GM-CSF), Rat Elastase ELISA Kit, and Rat Neprilysin ELISA Kit were purchased from MyBioSource, San Diego, US. Matrix metalloproteinase (MMP-1) ELISA kit was purchased from Lifespan Bioscience, North America.

Histopathological study. Skin specimens obtained from the rats' dorsal skin were fixed and embedded in paraffin for histopathological studies. Paraffin bees wax tissue blocks were prepared for sectioning at a thickness of four μ m by sledge microtome. The obtained tissue sections were collected on glass slides, de-paraffinized, and then stained by hematoxylin and eosin stain for examination using the light electric microscope (Optika B 150, Optika Microscopes, Italy).

Cutaneous irritation. The irritancy of the RM-LNC gels was evaluated according to the method previously described¹²². The dorsal side of the rats was shaved 24 h before the beginning of the experiment. The animals were divided into 6 groups each containing 6 rats: Group 1 served as control (no treatment), group 2 received 0.8% v/v aqueous formalin solution as a standard irritant¹²³, groups T1, T2, T3, and T4 received RHE, 4%-RM-LNC gel, 10% RM-LNC gel, and plain LNC gel. An amount of 100 mg gel (or formalin solution) was applied once daily for 72 h. The application sites were examined for edema and erythema at 24 and 72 h and graded (0–4), as shown in Table 9, according to a visual standard score¹²⁴; the final score represents the average of the 24 and 72 h readings. The primary irritancy index (PII) was determined for each preparation by adding the edema and erythema scores; the formulations were accordingly classified as non-irritant if PII < 2, irritant if PII = 2–5, and highly irritant if PII = 5–8.

Statistical analysis. The *invitro* data were compared using one-way analysis of variance, followed by multiple comparisons of Tukey–Kramer test using Graph Pad InStat® software (GraphPad4 Software, La Jolla, CA). The significance level was at $p < 0.05$. Data obtained from *in vivo* study were expressed as the mean of three experiments \pm the standard deviation (SD) or \pm the standard error of mean (SEM) and were analysed using one-way analysis of variance (ANOVA), followed by the least significant difference procedure using SPSS® software (SPSS, Inc., Chicago, Illinois, USA). Statistical differences yielding $p < 0.05$ were considered significant.

Conclusions

Bioactive natural products and plant extracts inspired by traditional medicine are increasingly expanding the anti-aging and photoprotective therapeutic arsenal especially with the increasing life expectancy and the green shift towards the use of natural health care products. With its content of phenolic diterpenes, triterpenoids, monoterpenoids, and long chain hydrocarbons, rosemary hexane extract demonstrated interesting *in vitro* anti-elastase, antioxidant, and wound healing properties associated with no cytotoxicity, representing a cost-effective and relatively safe anti-aging approach. *In silico* molecular modelling posed verbenone as the main constituent responsible for the anti-elastase activity of the extract through its significantly high docking score and favourable binding mode. The findings were further consolidated with *in vivo* results where *Rosmarinus officinalis* hexane extract, formulated in lipid nanocapsules-based mucoadhesive gel, provided UV-protection, restored the antioxidant biochemical state, decreased the level of inflammatory and wrinkling markers, and improved epidermal and dermal histological features in UV-irradiated rat model. The feasibility of synergy with known antioxidant and photoprotective natural products and the use of systemic photoprotection in conjunction with topical routes are yet to be explored.

Data availability

The data supporting this study are available upon request to Nehal Ibrahim (nehal.sabry@pharma.asu.edu.eg).

Received: 17 January 2022; Accepted: 12 July 2022

Published online: 30 July 2022

References

- Liu, T. *et al.* Recent advances in the anti-aging effects of phytoestrogens on collagen, water content, and oxidative stress. *Phytother. Res.* **34**, 435–447 (2020).
- Ahmed, I. A., Mikail, M. A., Zamakshshari, N. & Abdullah, A.-S.H. Natural anti-aging skincare: Role and potential. *Biogerontology* **21**, 293–310 (2020).
- Ferreira, M. S., Magalhães, M. C., Oliveira, R., Sousa-Lobo, J. M. & Almeida, I. F. Trends in the use of botanicals in anti-aging cosmetics. *Molecules* **26**, 3584 (2021).
- Hernandez, D. F., Cervantes, E. L., Luna-Vital, D. A. & Mojica, L. Food-derived bioactive compounds with anti-aging potential for nutraceutical and cosmeceutical products. *Crit. Rev. Food Sci. Nutr.* **61**, 3740–3755 (2021).
- Sim, Y. Y. & Nyam, K. L. Application of *Hibiscus cannabinus* L. (kenaf) leaves extract as skin whitening and anti-aging agents in natural cosmetic prototype. *Ind. Crops Prod.* **167**, 113491 (2021).
- Embuscado, M. E. Spices and herbs: Natural sources of antioxidants—a mini review. *J. Funct. Foods* **18**, 811–819 (2015).
- CBI Ministry of Foreign Affairs. <https://www.cbi.eu/market-information/natural-ingredients-cosmetics/trends>.
- Heinrich, M., Kufer, J., Leonti, M. & Pardo-de-Santayana, M. Ethnobotany and ethnopharmacology—Interdisciplinary links with the historical sciences. *J. Ethnopharmacol.* **107**, 157–160 (2006).
- González-Minero, F. J., Bravo-Díaz, L. & Ayala-Gómez, A. *Rosmarinus officinalis* L. (Rosemary): An ancient plant with uses in personal healthcare and cosmetics. *Cosmetics* **7**, 77 (2020).
- Borges, R. S., Ortiz, B. L. S., Pereira, A. C. M., Keita, H. & Carvalho, J. C. T. *Rosmarinus officinalis* essential oil: A review of its phytochemistry, anti-inflammatory activity, and mechanisms of action involved. *J. Ethnopharmacol.* **229**, 29–45 (2019).
- Ojeda-Sana, A. M., van Baren, C. M., Elechosa, M. A., Juárez, M. A. & Moreno, S. New insights into antibacterial and antioxidant activities of rosemary essential oils and their main components. *Food Control* **31**, 189–195 (2013).
- Diniz do Nascimento, L. *et al.* Bioactive natural compounds and antioxidant activity of essential oils from spice plants: New findings and potential applications. *Biomolecules* **10**, 988 (2020).
- Birtić, S., Dussort, P., Pierre, F.-X., Bily, A. C. & Roller, M. Carnosic acid. *Phytochemistry* **115**, 9–19 (2015).
- Abu-Al-Basal, M. A. Healing potential of *Rosmarinus officinalis* L. on full-thickness excision cutaneous wounds in alloxan-induced-diabetic BALB/c mice. *J. Ethnopharmacol.* **131**, 443–450 (2010).
- Ozarowski, M. *et al.* *Rosmarinus officinalis* L. leaf extract improves memory impairment and affects acetylcholinesterase and butyrylcholinesterase activities in rat brain. *Fitoterapia* **91**, 261–271 (2013).
- Ezzat, S. M., Salama, M. M., ElMeshad, A. N., Teaima, M. H. & Rashad, L. A. HPLC–DAD–MS/MS profiling of standardized rosemary extract and enhancement of its anti-wrinkle activity by encapsulation in elastic nanovesicles. *Arch. Pharmacol. Res.* **39**, 912–925 (2016).
- de Macedo, L. M. *et al.* Rosemary (*Rosmarinus officinalis* L., syn *Salvia rosmarinus* Spenn.) and its topical applications: A review. *Plants* **9**, 651 (2020).
- Ramadan, K. S., Khalil, O. A., Danial, E. N., Alnahdi, H. S. & Ayaz, N. O. Hypoglycemic and hepatoprotective activity of *Rosmarinus officinalis* extract in diabetic rats. *J. Physiol. Biochem.* **69**, 779–783 (2013).
- Park, M. *et al.* Carnosic acid, a phenolic diterpene from rosemary, prevents UV-induced expression of matrix metalloproteinases in human skin fibroblasts and keratinocytes. *Exp. Dermatol.* **22**, 336–341 (2013).
- Rahbardar, M. G., Amin, B., Mehri, S., Mirnajafi-Zadeh, S. J. & Hosseinzadeh, H. Anti-inflammatory effects of ethanolic extract of *Rosmarinus officinalis* L. and rosmarinic acid in a rat model of neuropathic pain. *Biomed. Pharmacother.* **86**, 441–449 (2017).
- Khan, A. *et al.* 1, 8-cineole (eucalyptol) mitigates inflammation in amyloid Beta toxicated PC12 cells: relevance to Alzheimer's disease. *Neurochem. Res.* **39**, 344–352 (2014).
- Huang, M.-T. *et al.* Inhibition of skin tumorigenesis by rosemary and its constituents carnosol and ursolic acid. *Can. Res.* **54**, 701–708 (1994).
- Inatani, R., Nakatani, N. & Fuwa, H. Antioxidative effect of the constituents of rosemary (*Rosmarinus officinalis* L.) and their derivatives. *Agric. Biol. Chem.* **47**, 521–528 (1983).
- Chen, Q., Shi, H. & Ho, C.-T. Effects of rosemary extracts and major constituents on lipid oxidation and soybean lipoxygenase activity. *J. Am. Oil Chem. Soc.* **69**, 999–1002 (1992).
- Tu, P. T. B. & Tawata, S. Anti-oxidant, anti-aging, and anti-melanogenic properties of the essential oils from two varieties of *Alpinia zerumbet*. *Molecules* **20**, 16723–16740 (2015).
- Thiviya, P., Gamage, A., Piumali, D., Merah, O. & Madhujith, T. Apiaceae as an important source of antioxidants and their applications. *Cosmetics* **8**, 111 (2021).
- Salem, M. A. *et al.* Coriander (*Coriandrum sativum* L.) essential oil and oil-loaded nano-formulations as an anti-aging potentiality via TGFβ/SMAD pathway. *Sci. Rep.* **12**, 1–15 (2022).
- Dzubak, P. *et al.* Pharmacological activities of natural triterpenoids and their therapeutic implications. *Nat. Prod. Rep.* **23**, 394–411 (2006).
- Ibrahim, S. A. & Li, S. K. Efficiency of fatty acids as chemical penetration enhancers: Mechanisms and structure enhancement relationship. *Pharm. Res.* **27**, 115–125 (2010).
- Ijaz, M. & Akhtar, N. Fatty acids based α-Tocopherol loaded nanostructured lipid carrier gel: In vitro and in vivo evaluation for moisturizing and anti-aging effects. *J. Cosmet. Dermatol.* **19**, 3067–3076 (2020).
- Tzima, K., Brunton, N. P. & Rai, D. K. Evaluation of the impact of chlorophyll removal techniques on polyphenols in rosemary and thyme by-products. *J. Food Biochem.* **44**, e13148 (2020).
- Ibrahim, N. & Moussa, A. Y. A comparative volatilomic characterization of Florence fennel from different locations: Antiviral prospects. *Food Funct.* **12**, 1498–1515 (2021).
- Heurtault, B., Saulnier, P., Pech, B., Proust, J.-E. & Benoit, J.-P. A novel phase inversion-based process for the preparation of lipid nanocarriers. *Pharm. Res.* **19**, 875–880 (2002).
- Huynh, N. T., Passirani, C., Saulnier, P. & Benoit, J. P. Lipid nanocapsules: A new platform for nanomedicine. *Int. J. Pharm.* **379**, 201–209 (2009).
- Li, Y. *et al.* Solar ultraviolet irradiation induces decorin degradation in human skin likely via neutrophil elastase. *PLoS ONE* **8**, e72563 (2013).
- Da Porto, C., Decorti, D. & Kikic, I. Flavour compounds of *Lavandula angustifolia* L. to use in food manufacturing: Comparison of three different extraction methods. *Food Chem.* **112**, 1072–1078 (2009).
- Erbas, S. & Baydar, H. Variation in scent compounds of oil-bearing rose (*Rosa damascena* Mill.) produced by headspace solid phase microextraction, hydrodistillation and solvent extraction. *Rec. Nat. Prod.* **10**, 555 (2016).

38. Mohamed, W. A., Abd-Elhakim, Y. M. & Farouk, S. M. Protective effects of ethanolic extract of rosemary against lead-induced hepato-renal damage in rabbits. *Exp. Toxicol. Pathol.* **68**, 451–461 (2016).
39. Medeiros, R., Otuki, M. F., Avellar, M. C. W. & Calixto, J. B. Mechanisms underlying the inhibitory actions of the pentacyclic triterpene α -amyryrin in the mouse skin inflammation induced by phorbol ester 12-O-tetradecanoylphorbol-13-acetate. *Eur. J. Pharmacol.* **559**, 227–235 (2007).
40. Santos, F. A. *et al.* Antihyperglycemic and hypolipidemic effects of α , β -amyryrin, a triterpenoid mixture from *Protium heptaphyllum* in mice. *Lipids Health Dis.* **11**, 98 (2012).
41. Navarrete, A., Trejo-Miranda, J. L. & Reyes-Trejo, L. Principles of root bark of *Hippocratea excelsa* (Hippocrateaceae) with gastroprotective activity. *J. Ethnopharmacol.* **79**, 383–388 (2002).
42. Oliveira, F. A. *et al.* Pentacyclic triterpenoids, α , β -amyryrins, suppress the scratching behavior in a mouse model of pruritus. *Pharmacol. Biochem. Behav.* **78**, 719–725 (2004).
43. Biskup, E., Gołębowski, M., Gniadecki, R., Stepnowski, P. & Lojkowska, E. Triterpenoid α -amyryrin stimulates proliferation of human keratinocytes but does not protect them against UVB damage. *Acta Biochim. Pol.* **59**, 255–260 (2012).
44. Wang, W.-H., Chuang, H.-Y., Chen, C.-H., Chen, W.-K. & Hwang, J.-J. Lupeol acetate ameliorates collagen-induced arthritis and osteoclastogenesis of mice through improvement of microenvironment. *Biomed. Pharmacother.* **79**, 231–240 (2016).
45. Chen, Y.-F. *et al.* *Balanophora spicata* and lupeol acetate possess antinociceptive and anti-inflammatory activities in vivo and in vitro. *Evid. Based Complem. Altern. Med.* **2012**, 371273 (2012).
46. Peixoto, J. A. B. *et al.* Comprehensive phenolic and free amino acid analysis of rosemary infusions: Influence on the antioxidant potential. *Antioxidants* **10**, 500 (2021).
47. Kontogianni, V. G. *et al.* Phytochemical profile of *Rosmarinus officinalis* and *Salvia officinalis* extracts and correlation to their antioxidant and anti-proliferative activity. *Food Chem.* **136**, 120–129 (2013).
48. Hossain, M. B., Rai, D. K., Brunton, N. P., Martin-Diana, A. B. & Barry-Ryan, C. Characterization of phenolic composition in Lamiaceae spices by LC-ESI-MS/MS. *J. Agric. Food Chem.* **58**, 10576–10581 (2010).
49. Ayoub, I. *et al.* Insights on the neuroprotective effects of *Salvia officinalis* L. and *Salvia microphylla* Kunth in memory impairment rat model. *Food Funct.* **13**, 2253–2268 (2022).
50. Almela, L., Sánchez-Muñoz, B., Fernández-López, J. A., Roca, M. J. & Rabe, V. Liquid chromatographic–mass spectrometric analysis of phenolics and free radical scavenging activity of rosemary extract from different raw material. *J. Chromatogr. A* **1120**, 221–229 (2006).
51. Linares, I. B. *et al.* Comparison of different extraction procedures for the comprehensive characterization of bioactive phenolic compounds in *Rosmarinus officinalis* by reversed-phase high-performance liquid chromatography with diode array detection coupled to electrospray time-of-flight mass spectrometry. *J. Chromatogr. A* **1218**, 7682–7690 (2011).
52. Tramontina, R. *et al.* Consolidated production of coniferol and other high-value aromatic alcohols directly from lignocellulosic biomass. *Green Chem.* **22**, 144–152 (2020).
53. El-Gazar, A. A., Emad, A. M., Ragab, G. M. & Rasheed, D. M. *Mentha pulegium* L. (Pennyroyal, Lamiaceae) extracts impose abortion or fetal-mediated toxicity in pregnant rats; evidenced by the modulation of pregnancy hormones, MiR-520, MiR-146a, TIMP-1 and MMP-9 protein expressions, inflammatory state, certain related signaling pathways, and metabolite profiling via UPLC-ESI-TOF-MS. *Toxins* **14**, 347 (2022).
54. Abdelaziz, S. *et al.* Phytochemical profile, antioxidant and cytotoxic potential of *Parkinsonia aculeata* L. growing in Saudi Arabia. *Saudi Pharm. J.* **28**, 1129–1137 (2020).
55. Zhang, J. *et al.* Screening active ingredients of rosemary based on spectrum-effect relationships between UPLC fingerprint and vasorelaxant activity using three chemometrics. *J. Chromatogr. B* **1134**, 121854 (2019).
56. Mena, P. *et al.* Phytochemical profiling of flavonoids, phenolic acids, terpenoids, and volatile fraction of a rosemary (*Rosmarinus officinalis* L.) extract. *Molecules* **21**, 1576 (2016).
57. Loussouarn, M. *et al.* Carnosic acid and carnosol, two major antioxidants of rosemary, act through different mechanisms. *Plant Physiol.* **175**, 1381–1394 (2017).
58. Seró, R. *et al.* Modified distribution in the polyphenolic profile of rosemary leaves induced by plant inoculation with an arbuscular mycorrhizal fungus. *J. Sci. Food Agric.* **99**, 2966–2973 (2019).
59. Zhao, L. *et al.* Simultaneous determination of oleanolic and ursolic acids in rat plasma by HPLC–MS: Application to a pharmacokinetic study after oral administration of different combinations of QingGanSanJie decoction extracts. *J. Chromatogr. Sci.* **53**, 1185–1192 (2015).
60. Chen, K., Ríos, J. J., Pérez-Gálvez, A. & Roca, M. Development of an accurate and high-throughput methodology for structural comprehension of chlorophylls derivatives. (I) Phytolated derivatives. *J. Chromatogr. A* **1406**, 99–108 (2015).
61. Shahinuzzaman, M. *et al.* In vitro antioxidant activity of *Ficus carica* L. latex from 18 different cultivars. *Sci. Rep.* **10**, 1–14 (2020).
62. Jadid, N. *et al.* in AIP Conference Proceedings, Vol. 1854 020019 (AIP Publishing LLC, 2017).
63. Sahu, R. K., Kar, M. & Routray, R. DPPH free radical scavenging activity of some leafy vegetables used by tribals of Odisha, India. *J. Med. Plants* **1**, 21–27 (2013).
64. Rašković, A. *et al.* Antioxidant activity of rosemary (*Rosmarinus officinalis* L.) essential oil and its hepatoprotective potential. *BMC Complem. Altern. Med.* **14**, 225 (2014).
65. Qanash, H. *et al.* Anticancer, antioxidant, antiviral and antimicrobial activities of Kei Apple (*Dovyalis caffra*) fruit. *Sci. Rep.* **12**, 1–15 (2022).
66. Sridhar, K. & Charles, A. L. In vitro antioxidant activity of Kyoho grape extracts in DPPH and ABTS assays: Estimation methods for EC50 using advanced statistical programs. *Food Chem.* **275**, 41–49 (2019).
67. Sağlam, H., Pabuçcuoğlu, A. & Kıvçak, B. Antioxidant activity of *Vitex agnus-castus* L. extracts. *Phytother. Res.* **21**, 1059–1060 (2007).
68. Dudonne, S., Vitrac, X., Coutiere, P., Woillez, M. & Mérillon, J.-M. Comparative study of antioxidant properties and total phenolic content of 30 plant extracts of industrial interest using DPPH, ABTS, FRAP, SOD, and ORAC assays. *J. Agric. Food Chem.* **57**, 1768–1774 (2009).
69. Thaipong, K., Boonprakob, U., Crosby, K., Cisneros-Zevallos, L. & Byrne, D. H. Comparison of ABTS, DPPH, FRAP, and ORAC assays for estimating antioxidant activity from guava fruit extracts. *J. Food Compos. Anal.* **19**, 669–675 (2006).
70. Furger, C. Live cell assays for the assessment of antioxidant activities of plant extracts. *Antioxidants* **10**, 944 (2021).
71. Oikarinen, A. Aging of the skin connective tissue: how to measure the biochemical and mechanical properties of aging dermis. *Photodermatol. Photoimmunol. Photomed.* **10**, 47 (1994).
72. Uitto, J. The role of elastin and collagen in cutaneous aging: Intrinsic aging versus photoexposure. *JDD* **7**, s12 (2008).
73. Miri, A. K., Heris, H. K., Mongeau, L. & Javid, F. Nanoscale viscoelasticity of extracellular matrix proteins in soft tissues: A multiscale approach. *J. Mech. Behav. Biomed. Mater.* **30**, 196–204 (2014).
74. Vayalil, P. K., Mittal, A., Hara, Y., Elmets, C. A. & Katiyar, S. K. Green tea polyphenols prevent ultraviolet light-induced oxidative damage and matrix metalloproteinases expression in mouse skin. *J. Invest. Dermatol.* **122**, 1480–1487 (2004).
75. Suganuma, K., Nakajima, H., Ohtsuki, M. & Imokawa, G. Astaxanthin attenuates the UVA-induced up-regulation of matrix-metalloproteinase-1 and skin fibroblast elastase in human dermal fibroblasts. *J. Dermatol. Sci.* **58**, 136–142 (2010).
76. Esser, P. R. *et al.* Contact sensitizers induce skin inflammation via ROS production and hyaluronic acid degradation. *PLoS ONE* **7**, e41340 (2012).

77. Takeuchi, H., Gomi, T., Shishido, M., Watanabe, H. & Suenobu, N. Neutrophil elastase contributes to extracellular matrix damage induced by chronic low-dose UV irradiation in a hairless mouse photoaging model. *J. Dermatol. Sci.* **60**, 151–158 (2010).
78. Mitaine-Offer, A.-C., Hornebeck, W., Sauvain, M. & Zèches-Hanrot, M. Triterpenes and phytosterols as human leucocyte elastase inhibitors. *Planta Med.* **68**, 930–932 (2002).
79. Kim, Y.-J., Uyama, H. & Kobayashi, S. Inhibition effects of (+)-catechin–aldehyde polycondensates on proteinases causing proteolytic degradation of extracellular matrix. *Biochem. Biophys. Res. Commun.* **320**, 256–261 (2004).
80. Givol, O. *et al.* A systematic review of *Calendula officinalis* extract for wound healing. *Wound Repair Regen.* **27**, 548–561 (2019).
81. Fronza, M., Heinzmann, B., Hamburger, M., Laufer, S. & Merfort, I. Determination of the wound healing effect of *Calendula* extracts using the scratch assay with 3T3 fibroblasts. *J. Ethnopharmacol.* **126**, 463–467 (2009).
82. Ahmed, H.M. & Babakir-Mina, M. Investigation of rosemary herbal extracts (*Rosmarinus officinalis*) and their potential effects on immunity. *Phytother. Res.* (2020).
83. Shrestha, S., Song, Y. W., Kim, H., Lee, D. S. & Cho, S. K. Sageone, a diterpene from *Rosmarinus officinalis*, synergizes with cisplatin cytotoxicity in SNU-1 human gastric cancer cells. *Phytomedicine* **23**, 1671–1679 (2016).
84. Cheung, S. & Tai, J. Anti-proliferative and antioxidant properties of rosemary *Rosmarinus officinalis*. *Oncol. Rep.* **17**, 1525–1531 (2007).
85. Pérez-Sánchez, A. *et al.* Rosemary (*Rosmarinus officinalis*) extract causes ROS-induced necrotic cell death and inhibits tumor growth in vivo. *Sci. Rep.* **9**, 1–11 (2019).
86. Golgi, S. A. Patent evaluation: Uses of verbenone and verbenone cyclodextrin complexes as anti-elastase drugs. *Curr. Opin. Therapeutic Patents* **3**, 1237–1238 (1993).
87. Abdel-Mottaleb, M.M.A., Neumann, D. & Lamprecht, A. Lipid nanocapsules for dermal application: A comparative study of lipid-based versus polymer-based nanocarriers. *Eur. J. Pharm. Biopharm.* In Press, Corrected Proof (2011).
88. Sasso, M. S. *et al.* Low dose gemcitabine-loaded lipid nanocapsules target monocytic myeloid-derived suppressor cells and potentiate cancer immunotherapy. *Biomaterials* **96**, 47–62 (2016).
89. Valcourt, C. *et al.* Synergistic interactions between doxycycline and terpenic components of essential oils encapsulated within lipid nanocapsules against gram negative bacteria. *Int. J. Pharm.* **498**, 23–31 (2016).
90. Abbas, H., Kamel, R. & El-Sayed, N. Dermal anti-oxidant, anti-inflammatory and anti-aging effects of Compritol ATO-based Resveratrol colloidal carriers prepared using mixed surfactants. *Int. J. Pharm.* **541**, 37–47 (2018).
91. Shetty, P. K. *et al.* Development and evaluation of sunscreen creams containing morin-encapsulated nanoparticles for enhanced UV radiation protection and antioxidant activity. *Int. J. Nanomed.* **10**, 6477–6491 (2015).
92. Kamel, R. & Abbas, H. A. Self-assembled carbohydrate hydrogels for prolonged pain management. *Pharm. Dev. Technol.* **18**, 990–1004 (2013).
93. Vonarbourg, A., Saulnier, P., Passirani, C. & Benoit, J. P. Electrokinetic properties of noncharged lipid nanocapsules: Influence of the dipolar distribution at the interface. *Electrophoresis* **26**, 2066–2075 (2005).
94. Manconi, M. *et al.* Viscoelastic properties of concentrated dispersions in water of soy lecithin. *Colloids Surf. A* **222**, 141–145 (2003).
95. Lamprecht, A., Bouligand, Y. & Benoit, J.-P. New lipid nanocapsules exhibit sustained release properties for amiodarone. *J. Control. Release* **84**, 59–68 (2002).
96. Tawfik, M.S., Abdel-Ghaffar, K.A., Gamal, A.Y., El-Demerdash, F.H. & Gad, H.A. Lycopene solid lipid microparticles with enhanced effect on gingival crevicular fluid protein carbonyl as a biomarker of oxidative stress in patients with chronic periodontitis. *J. Liposome Res.* 1–33 (2019).
97. Gad, H.A., Kamel, A.O., Ezzat, O.M., El Dessouky, H.F. & Sammour, O.A. Doxycycline hydrochloride-metronidazole solid lipid microparticles gels for treatment of periodontitis: development, in-vitro and in-vivo clinical evaluation. *Expert Opinion Drug Deliv.* 1–11 (2017).
98. Gad, H. A., El-Nabarawi, M. A. & Abdel-Hady, S. S. Formulation and evaluation of secnidazole or doxycycline dento-oral gels. *Drug Dev. Ind. Pharm.* **34**, 1356–1367 (2008).
99. Eff, A. R. Y., Rahayu, S. T., Saraswati, H. & Mun'im, A. Formulation and evaluation of sunscreen gels containing mangiferin isolated from *Phaleria macrocarpa* fruits. *Int. J. Pharm. Invest.* **9**, 141–145 (2019).
100. Kamel, R. & Mostafa, D. M. Rutin nanostructured lipid cosmeceutical preparation with sun protective potential. *J. Photochem. Photobiol., B* **153**, 59–66 (2015).
101. Debacq-Chainiaux, F., Leduc, C., Verbeke, A. & Toussaint, O. (2012).
102. da Silva, K. A. *et al.* Activation of cannabinoid receptors by the pentacyclic triterpene α , β -amyryn inhibits inflammatory and neuropathic persistent pain in mice. *Pain* **152**, 1872–1887 (2011).
103. Wang, L.-C. *et al.* An integrated proteomics and bioinformatics approach reveals the anti-inflammatory mechanism of carnosic acid. *Front. Pharmacol.* **9**, 370 (2018).
104. Maione, F. *et al.* Anti-inflammatory and analgesic activity of carnosol and carnosic acid in vivo and in vitro and in silico analysis of their target interactions. *Br. J. Pharmacol.* **174**, 1497–1508 (2017).
105. Lai, C.-S. *et al.* Rosmanol potently inhibits lipopolysaccharide-induced iNOS and COX-2 expression through downregulating MAPK, NF- κ B, STAT3 and C/EBP signaling pathways. *J. Agric. Food Chem.* **57**, 10990–10998 (2009).
106. Ganceviciene, R., Liakou, A. I., Theodoridis, A., Makrantonaki, E. & Zouboulis, C. C. Skin anti-aging strategies. *Dermatoendocrinology* **4**, 308–319 (2012).
107. Abbas, H. & Kamel, R. Potential role of resveratrol-loaded elastic sorbitan monostearate nanovesicles for the prevention of UV-induced skin damage. *J. Liposome Res.* **30**, 45–53 (2020).
108. Imokawa, G. Epithelial–mesenchymal interaction mechanisms leading to the over-expression of neprilysin are involved in the UVB-induced formation of wrinkles in the skin. *Exp. Dermatol.* **25**, 2–13 (2016).
109. Lopez, V. C., Hadgraft, J. & Snowden, M. The use of colloidal microgels as a (trans) dermal drug delivery system. *Int. J. Pharm.* **292**, 137–147 (2005).
110. Mengoni, E. S. *et al.* Suppression of COX-2, IL-1 β and TNF- α expression and leukocyte infiltration in inflamed skin by bioactive compounds from *Rosmarinus officinalis* L. *Fitoterapia* **82**, 414–421 (2011).
111. Ibrahim, N. & Moussa, A. Y. Comparative metabolite profiling of *Callistemon macropunctatus* and *Callistemon subulatus* volatiles from different geographical origins. *Ind. Crops Prod.* **147**, 112222 (2020).
112. Boly, R., Lamkani, T., Lompo, M., Dubois, J. & Guissou, I. DPPH free radical scavenging activity of two extracts from *Agelanthus dodoneifolius* (Loranthaceae) leaves. *Int. J. Toxicol. Pharmacol. Res.* **8**, 29–34 (2016).
113. Arnao, M. B., Cano, A. & Acosta, M. The hydrophilic and lipophilic contribution to total antioxidant activity. *Food Chem.* **73**, 239–244 (2001).
114. Benzie, I. F. & Strain, J. J. The ferric reducing ability of plasma (FRAP) as a measure of “antioxidant power”: The FRAP assay. *Anal. Biochem.* **239**, 70–76 (1996).
115. El-Hamoly, T. *et al.* Activation of poly (ADP-ribose) polymerase-1 delays wound healing by regulating keratinocyte migration and production of inflammatory mediators. *Mol. Med.* **20**, 363–371 (2014).
116. Denizot, F. & Lang, R. Rapid colorimetric assay for cell growth and survival: Modifications to the tetrazolium dye procedure giving improved sensitivity and reliability. *J. Immunol. Methods* **89**, 271–277 (1986).

117. El-Sheridy, N. A., Ramadan, A. A., Eid, A. A. & El-Khordagui, L. K. Itraconazole lipid nanocapsules gel for dermatological applications: In vitro characteristics and treatment of induced cutaneous candidiasis. *Colloids Surf., B* **181**, 623–631 (2019).
118. Gad, H. A., Abd El-Rahman, F. A. A. & Hamdy, G. M. Chamomile oil loaded solid lipid nanoparticles: A naturally formulated remedy to enhance the wound healing. *J. Drug Deliv. Sci. Technol.* **50**, 329–338 (2019).
119. Kuo, Y.-H., Chen, C.-W., Chu, Y., Lin, P. & Chiang, H.-M. In vitro and in vivo studies on protective action of N-phenethyl caffeamide against photodamage of skin. *PLoS ONE* **10**, e0136777 (2015).
120. Jagetia, G. C., Venkatesha, V. & Reddy, T. K. Naringin, a citrus flavonone, protects against radiation-induced chromosome damage in mouse bone marrow. *Mutagenesis* **18**, 337–343 (2003).
121. Kumar, D. *et al.* Association between sperm DNA integrity and seminal plasma antioxidant levels in health workers occupationally exposed to ionizing radiation. *Environ. Res.* **132**, 297–304 (2014).
122. Draize, J. H. Methods for the study of irritation and toxicity of substances applied topically to the skin and mucous membranes. *J. Pharmacol. Exp. Ther.* **82**, 377–390 (1944).
123. Aboelwafa, A. A., El-Setouhy, D. A. & Elmeshad, A. N. Comparative study on the effects of some polyoxyethylene alkyl ether and sorbitan fatty acid ester surfactants on the performance of transdermal carvedilol proniosomal gel using experimental design. *AAPS PharmSciTech* **11**, 1591–1602 (2010).
124. Blume-Peytavi, U. *et al.* Cutaneous lycopene and β -carotene levels measured by resonance Raman spectroscopy: High reliability and sensitivity to oral lactolycopene deprivation and supplementation. *Eur. J. Pharm. Biopharm.* **73**, 187–194 (2009).

Acknowledgements

Nehal Ibrahim expresses deep gratitude to Professor Omayma Eldahshan (Ain Shams University, Cairo, Egypt) for continuous support.

Author contributions

Conceptualization: N. I., H. A. G., Methodology: N. I., H. A., H. A. G., Formal analysis and investigation: N. I., H. A., H. A. G., Writing-preparation of the original draft: N. I., H. A., H. A. G., Writing-proofreading and editing: N. S. E., H. A. G., Data curation: N. I., H. A., H. A. G.

Funding

Open access funding provided by The Science, Technology & Innovation Funding Authority (STDF) in cooperation with The Egyptian Knowledge Bank (EKB).

Competing interests

The authors declare no competing interests.

Additional information

Correspondence and requests for materials should be addressed to N.I. or H.A.G.

Reprints and permissions information is available at www.nature.com/reprints.

Publisher's note Springer Nature remains neutral with regard to jurisdictional claims in published maps and institutional affiliations.



Open Access This article is licensed under a Creative Commons Attribution 4.0 International License, which permits use, sharing, adaptation, distribution and reproduction in any medium or format, as long as you give appropriate credit to the original author(s) and the source, provide a link to the Creative Commons licence, and indicate if changes were made. The images or other third party material in this article are included in the article's Creative Commons licence, unless indicated otherwise in a credit line to the material. If material is not included in the article's Creative Commons licence and your intended use is not permitted by statutory regulation or exceeds the permitted use, you will need to obtain permission directly from the copyright holder. To view a copy of this licence, visit <http://creativecommons.org/licenses/by/4.0/>.

© The Author(s) 2022